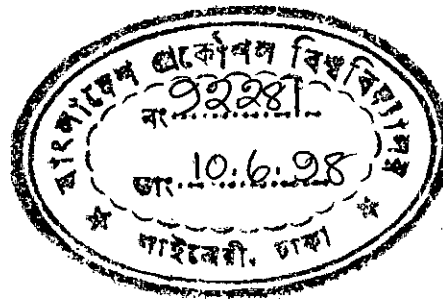# WIND TURBINE POWER SYSTEM SIMULATION FOR USE IN REMOTE AREAS OF BANGLADESH

By

MOHAMMAD ALI JINNAH

This thesis is submitted to the Department of Mechanical Engineering in partial fulfilment of the requirements for the degree of
Master of Science
in
Mechanical Engineering

BANGLADESH UNIVERSITY OF ENGINEERING AND TECHNOLOGY DHAKA-1000, BANGLADESH.
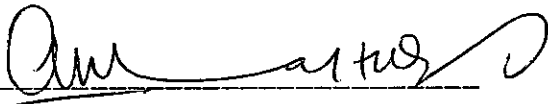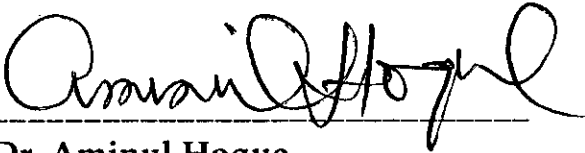
FEBRUARY 1998

The thesis titled "WIND TURBINE POWER SYSTEM SIMULATION FOR USE IN REMOTE AREAS OF BANGLADESH", submitted by Mohammad Ali Jinnah, Roll no. 921437F, Registration no. 86438 of M.Sc. Engineering (Mechanical) has been accepted as satisfactory in partial fulfillment of the requirement for the degree of Master of Science in Mechanical Engineering on 18th February, 1998

BOARD OF EXAMINERS

1. _____

   Dr. Muhammad Mahbubul Alam   **Chairman**
   Associate Professor   (Supervisor)
   Dept. of Mech. Engg.
   BUET, Dhaka.

2. _____

   Dr. A. M. Aziz-ul-Huq   **Member**
   Professor & Head   (Ex-officio)
   Dept. of Mech. Engg.
   BUET, Dhaka.

3. _____

   Dr. Md. Quamrul Islam   **Member**
   Professor
   Dept. of Mech. Engg.
   BUET, Dhaka.

4. _____
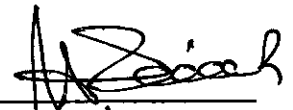
   Dr. Aminul Hoque   **Member**
   Professor   (External)
   Dept. of EEE. Engg.
   BUET, Dhaka.

CERTIFICATE OF RESEARCH

This to certify that the work presented in this thesis is the outcome of the investigation carried out by the candidate under the supervision of Dr. Muhammad Mahbubul Alam in the Department of Mechanical Engineering, BUET, Dhaka and it has not been submitted anywhere for any award of degree or diploma.

_____
Supervisor

_____
Candidate

ACKNOWLEDGEMENTS

ABSTRACT

This thesis present a procedure for the performance characteristics analysis of horizontal axis wind turbines. The wind turbine is tested by tunnel air at different air velocity to determine power coefficient, torque coefficient and their variations with respect to tip speed ratio. Based on this test data, the wind turbine is replaced by an electric motor whose performance is closed to the wind turbine. Thus this simulated system can be used for research activities at the indoor laboratory conditions. Various wind-powered models matched for water pumping or electricity generation can then be developed without weather dependent outdoor experimentation.

CONTENTS

LIST OF SYMBOLS

a $\dfrac{B}{2} \cdot \dfrac{R-r}{R \sin \phi}$

A   turbine disc area, πR^2

A_1 cross sectional area of incoming wind

A_2 wake cross-sectional area

B   number of blades

C   chord of the blades

C_D blade drag coefficient, $\dfrac{dD}{\frac{1}{2}\rho\, C V_r^2\, dr}$

C_L blade lift coefficient, $\dfrac{dL}{\frac{1}{2}\rho\, C V_r^2\, dr}$

C_P power coefficient, $\dfrac{P}{\frac{1}{2}\rho\, A V_\infty^3}$

C_T torque coefficient, $\dfrac{T}{\frac{1}{2}\rho\, A V_\infty^2 R}$

dA   blade element area, C dr

D   drag force

E_b back e.m.f.

f   axial interference factor

f'   tangential interference factor

F_f correction factor

F_{hub} hub loss factor

F_R Resultant force

F_{tip} tip loss factor

I	electric current
I_a	armature current
P	power
P^+	pressure immediately in front of the rotor
P^-	pressure immediately behind the rotor
P_a	atmospheric pressure
P_∞	free stream pressure
r	local blade radius
r_{hub}	hub radius
R	rotor radius
R_a	armature resistance
U	wind speed through the turbine
V	wind velocity
V_∞	Undisturbed wind velocity
V_c	electric voltage
V_r	relative wind velocity
t	atmospheric temperature

SUBSCRIPTS

a	axial
D	drag
L	lift
max.	maximum
min.	minimum
P	power
T	torque
r	local
ref	reference
S_t	starting

GREEK LETTERS

α	angle of attack
ϕ	angle of relative wind velocity
σ	solidity
π	pi
ω	angular velocity
ν	kinematic viscosity of the fluid
ρ	density
λ	tip speed ratio

CHAPTER-1

INTRODUCTION
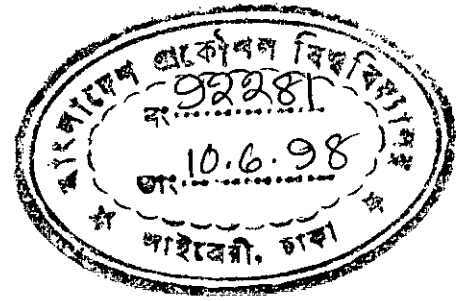
Wind energy is now being considered as one of the cleanest renewable energies used throughout the world. Scope of utilization of wind powered equipments in Bangladesh can be of variant types such as lifting water from nearby river or sea for irrigation, salt farming, prawn farms and electricity generation for remote areas. In present world, energy crisis is a vital problem. There are many sources of energy such as gas, petroleum oils, solar, tidal, wind energy etc. The wind energy is one of the cheapest source of energy. Wind energy can be converted into mechanical energy through wind turbine. Environmental pollution and public health hazard due to energy conversion may be avoided if we exact energy from wind. The success of wind energy as an alternate energy source is obviously a direct function of the economics of production of wind power machines. In this regard, the role of improved power output through the development of better aerodynamic performance offer some potential return. Various studies have indicated that wind energy has the potential to make significant contributions to the national needs. Therefore, our nation is interestedto new cheapest energy source and to justify their practicability. The studies reported in this thesis presents a procedure for the performance characteristics analysis of horizontal axis wind turbine. In the first part of the program, a wind turbine is tested by tunnel air. The air flows through the wind tunnel with high velocity when the propeller of the wind tunnel rotate and this high velocity air is controlled to rotate the wind turbine. The wind turbine is tested at different air velocity to determine coefficient of power, torque coefficient and their variation with respect to tip speed ratio. Based on this test data, the wind turbine is replaced by an electric motor whose performance is closed to the wind turbine. By

these simulated system, the wind powered machine is developed to use in practical purpose. These development of the wind-power utilization systems can remove the difficulties of the wind power utilization in the field of irrigation and electricity generation. In irrigation system, wind-powered water pumps can be used where sufficient wind energy is available. Since substantial wind energy is available along the coastal regions of Bangladesh, wind powered pumping systems using direct mechanical coupling between a water pump and a wind turbine or another simulated system can be used in those areas. Generation of electricity by wind turbine is also feasible in some rural areas. The electric energy can be stored by storage device when a strong wind energy is available and these stored energy can be used for practical purpose when the wind flow falls.

1.1   HISTORICAL DEVELOPMENT

The history of wind power utilization is very long. However, its practical use has so far been almost neglected, mainly because of the instability of power supply for energy intensive modern society. Because of its small energy density and extreme fluctuation, wind can not produce a constant power supply unless it has appropriate strength with proper controlling devices.

The proverb saying that history repeats itself can be applied to the present worldwide energy situation as highlighted by the recent debate on the energy crisis. Recently wind power is being re-evaluated as a new potential source of power generation, irrigation and water supply.

Many different windmill designs have been constructed to extract power from the wind. The earliest known references to windmills relate to a Persian millwright in 644 A.D., as depicted in Figure 1.1, and to windmills is Seistan, Persia, in 915 A.D. [1]. These early windmills, which were used for moving water, consisted of several sails that rotated on a vertical axis. Later, horizontal-axis windmills, consisting of upto ten wooden booms, rigged with jib sails, were developed. Such primitive types of windmills are still found in use today in many Mediterranean regions.

By the eleventh century A.D., windmills were in extensive use in the Middle East and were introduced to Europe in the thirteenth century by returning Crusaders. During that time in Europe, many horizontal axis windmills had been constructed for grinding grains and raising water.
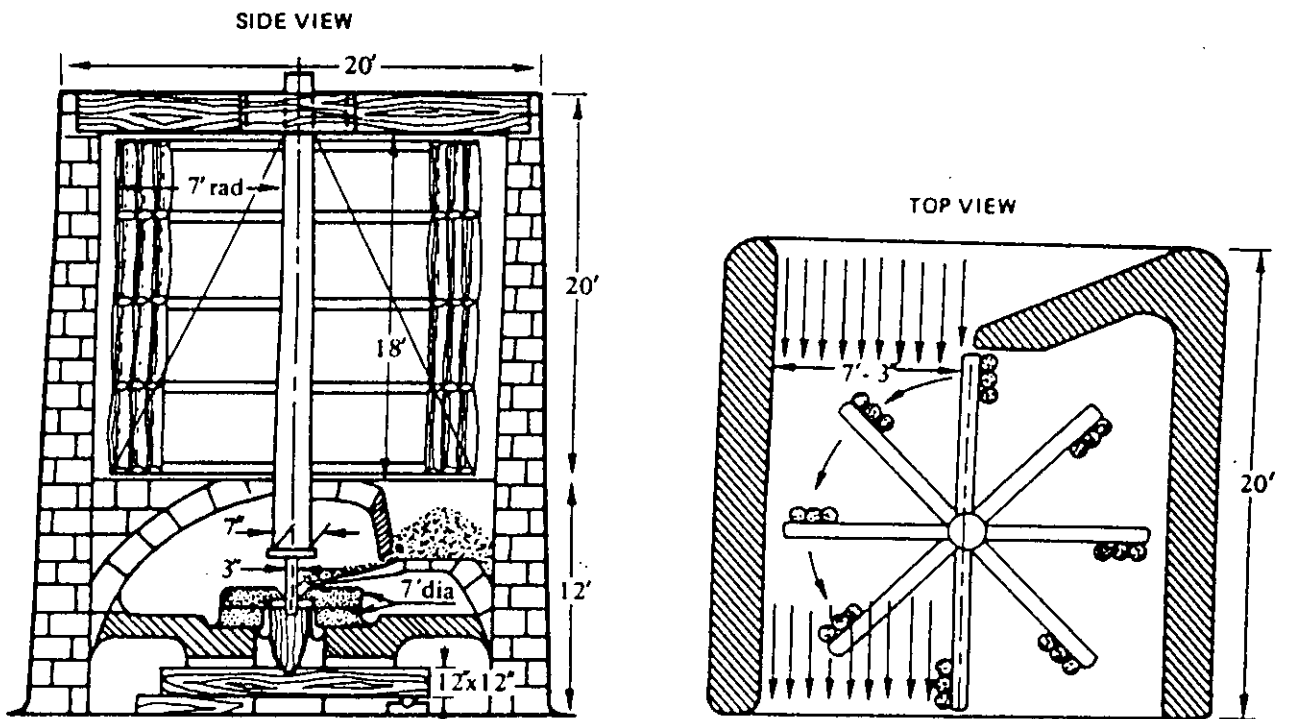
SIDE VIEW

TOP VIEW

Figure 1.1 : Persian Vertical Axis Windmill.

4

In the fourteenth century, the Dutch had taken the lead in improving the design of windmills and used them extensively thereafter for draining the marshes and lakes of Rhine river delta. The first oil mill was built in Holland in 1582, and in 1586 the first paper mill was constructed to meet the enormous demand for paper that resulted from the invention of the printing press. At the end of the sixteenth century, saw mills are introduced to process timber imported from the Baltic regions. By the middle of the nineteenth century, some 9000 windmills were being used in the Netherlands for a wide variety of purposes. The Dutch introduced many improvements in the design of windmills and, in particular, the rotors. By the sixteenth century, the primitive jib sails on wooden booms had given way to sails. The sails were typically constructed from sail cloth stretched over a wooden frame. The individual sails were flat planes and inclined at a constant angle to the direction of rotation. More modern designs substituted sheet metal for the cloth sails, and introduced various types of the rotor in heavy weather. With the introduction of the steam engine, during the industrial revolution, the use of wind power in Holland started to decline, and by the turn of the twentieth century, only about 2500 windmills were still in operation in the Netherlands. By 1960, fewer than 1000 were still in working condition. Since the mid-nineteenth century, more than six-million small multi-bladed windmills, providing power outputs of less than 1 hp each in an average wind, have been built and used in the USA to pump water, generate electricity and perform similar functions. During the early part of the twentieth century, two quite different vertical designs were developed. One of the designs, known as the Savonius Rotor was formed by cutting a cylinder into two semi-cylindrical surfaces, moving these surfaces sideways along the cutting plane to form a rotor with cross-section in the form of the letter "S" placing a shaft in the center of the rotor, and closing the end surfaces with circular end plates as shown in Fig. 1.2. The other vertical windmill design, patented in 1927

5

by George Darrieus consisted of two thin air foils with one end mounted on the lower end of a vertical shaft and the other end mounted on the upper end of the same shaft, sketched in Fig. 1.3.

Palmer Putnam had constructed a windmill with the help of the S. Morgan Smith Company of New York, Pennsylvania using NACA4418 as shown in the Figure 1.4 and operated the plant in the early 1940. The two bladed, 175 ft. diameter, propeller type rotor, weighed 16 tons and rotated at a constant speed of 28 rpm to produce upto 1.25 Megawatts (MW) of power, operated during the period from 1941 to 1949.

In Denmark, by the end of nineteenth century, there were about 2500 industrial windmills in operation, supplying a total of about 40,000 hp or 30 MW; i.e. about 25% of the total power available to Danish industry at that time [2]. In addition, approximately 4600 windmills were also being used on about 2% of the Danish for various applications, including threshing, milling of grains, and water pumping. By the 1930's the number of industrial windmills had declined to about 1000 but the number of farm units had increased to about 1600. During world war 1, the Danish developed and operated a number of various types of large-scale wind machines for producing electricity. The number of these machines increased from 16 in the summer of 1940, to 88 by the beginning of 1944. After world war II, the number of operating machines started to decrease and at the end of 1947, they dropped to 57. The decrease continued in the 1950's and by the end of that decade the production of electricity by wind machine was being conducted only on an experimental basis in Denmark, with units rated at 12, 45 and 200 kW. The 200 kW Gedser mill, which was the latest in this series, was operated until 1968. After the energy crunch of 1973, the 200 kW Gedser mill was refurbished, and in 1977 it was put back into service. In 1931, the Russians built an advanced 100 kW wind turbine near Yalta on the Black
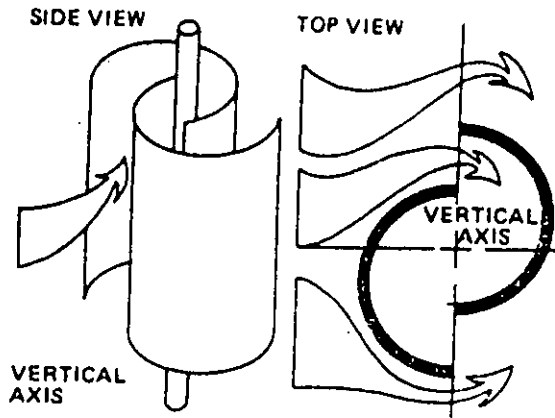
Figure 1.2 : Savonius Rotor
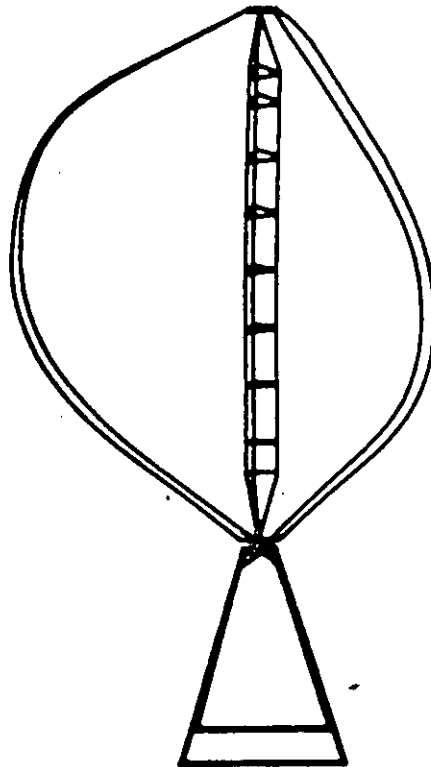
Figure 1.3 : Darrieus Rotor

7

sea. The annual output of this machine was found to be about 280,000 kWh per year.

In England, in the late 1940's and during the 1950's considerable work was done on wind-powered electrical generation plants. In 1950, the North Sealand Hydroelectric Board commissioned the John Brown Company an experimental wind turbine or Cape Costa in the Orkney Islands. This unit was designed to generate 100 kW in winds of 35 mph. It operated for short periods in 1955, coupled to a direct powered electric utility network, but was shut down because of operational problems. In the 1950's the Enfold Cable Company built a wind-powered generator designed by a Frenchman named Andreau shown in Figure 1.5. This machine was operated at St. Albans, England, and later in Algeria. It was designed to generate 100 kW of ac power in the wind speed of 30 mph . The machine was particularly interesting in that, unlike conventional wind turbines, it used air rather than gears to transmit the propeller power to the generator. The propellers blades were hollow, and when they rotated, they acted as centrifugal pumps. The air entered through the ports in the lower part of the tower; passed through an air turbine which turned the electric generator; went up through the tower; and went out the hollow tips of the blades. The efficiency of the unit was found to be low compared to more conventional horizontal-axis wind-powered rotors. The main advantage of this system was that the power generating equipment was not supported shaft.

The history of practical windmills in Japan started at the beginning of the Meiji era, in the early 1880's. However, windmills as toys or ornaments have a rather long history for example, there were famous paper windmills at Gofukuji tample in shiojiri of Nagano prefecture. These paper windmills, which had a diameter of 0.5m, had sold at festivals for 200 years. Regarding their use in advertising, there was a famous

8
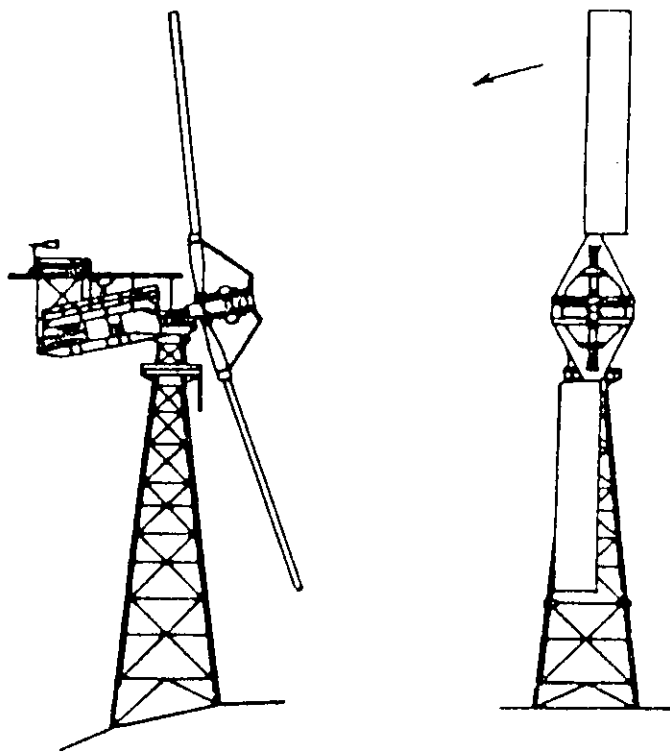
Figure 1.4 : Smith-Putnam Wind Turbine.

AIR VENT

PROPELLER

AIR VENT

TURBINE

GENERATOR — AIR INTAKES
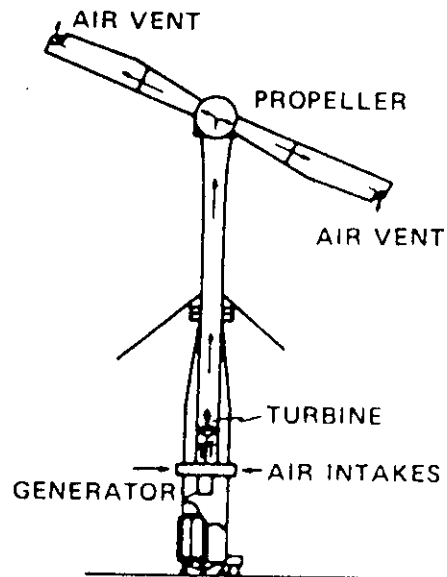
Figure 1.5 : Enfield-Andreau Wind Energy Conversion System.

9

windmill on the roof of a buckwheat noodle shop in Zoshigaya of Edo in the Meiwa era (1970's). However, the history of practical windmills in Japan started when foreigners from the USA and Europe visited this country at the beginning of the Meiji era, in the early 1880's. The built windmills in various parts of Japan as water moving devices. In 1887, the first America-style wooden windmill was installed for pumping water at an American run stock-farm. Then, as the prime mover of water supply systems, windmills were used in the foreigners' residential areas and at mission schools etc, mainly in the Keihin and Hanshin (Osaka-Kobe) areas. Thereafter, until the mid 1920's the windmills were mainly imported from the USA and Germany. They were primarily used for water supply and pumping. Besides these imported windmills, there were irrigation windmills worthy of special mention. Since the end of the Meiji era (1900's) simple wooden windmills were built by the local carpenter or blacksmith at relatively low cost. A total of several thousands windmills were operated in Nagano, Ibaraki, Chiba, Osaka and Aichi Prophetesses. These were used for a long time until just after world war II, in the 1950's. On the other hand, wind-powered electric generation had not been so active, except for the wind turbine which was widely used mainly by pioneering farmers in Hokkaido after world war II. History tells us that these successful wind power utilizations were due not only to the natural environmental conditions but mainly to the social conditions.

The French built and operated several large wind-powered electric generators in the period from 1958 to 1966. These included three horizontal-axis units, each with three propeller-type blades. A unit of this kind was operated intermittently near Paris from 1958 to 1963. This unit was designed to generate 800 kW in winds of 37 mph. Two other units were constructed at St. Remy-des-landes in Souther France. The small unit had a 70 feet diameter rotor operated at 56 rpm. The larger of these two units was rated at 1000 kW in winds of 37 mph and weighed 96 tons, excluding the

tower. The French also built and tested several experimental vertical-axis panemonas during these period.

It had been estimated that the number of windmills in use in Germany were about 18000 in 1895, 17000 in 1907, 11400 in 1914 and between 4000 to 5000 in 1933. The Germans introduced a number of improvements in the design of wind-powered generators, including light-weight-constant speed rotors that were controlled by variable pitch propeller blades with swept diameters as large as 110 feet. These machines used light-weight, composite carbon-epoxy or composite fiberglass-epoxy blades, with the generator mounted on a tower consisting of a small-diameter hollow-pipe. The largest unit generated 100 kW in 18 mph wind speed. The units operated successfully for more than 4000 hours during the period from 1957 to 1968.

Recently, large wind energy conversion systems have been built and tested in a number of countries around the world. But the problem has been that the installation cost per kilowatt has been too high when composed with the costs of other methods of producing electric power. In addition, because of wind variability, some of energy storage must also be considered. Today's increasing cost of fuel, coupled with potential fuel scarcities, has provoked the re-examination of wind energy as a future source of power.

1.2 AIM OF THE THESIS

The studies reported in this thesis present a procedure for the performance characteristics analysis of horizontal axis wind turbines. In the first part of the program, a wind turbine is tested by tunnel air. The air flows through the wind tunnel with high velocity and this high velocity air is controlled to rotate the wind turbine. The wind turbine is tested at different air velocity to determine power coefficient (C_p), torque coefficient (C_T), and C_p-λ, C_T-λ characteristics.

Based on this test data, the wind turbine is replaced by an electric motor whose performance is closed to the wind turbine. By these simulated system, the wind power machine is developed to use in practical purpose. These development of the wind-power utilization systems can remove the difficulties of the wind power utilization in the field of irrigation and electricity generation. In irrigation system wind-powered water pumps can be used where sufficient wind speed is available. Since substantial wind energy is available along the coastal regions of Bangladesh, wind-powered pumping systems using direct mechanical coupling between a water pump and a wind turbine or another simulated system can be used in those areas. Generation of electricity by wind turbine is also feasible in some rural area. The electric energy can be stored by storage device when a strong wind speed is available and these stored energy can be used for practical purpose when wind speed falls.

Finally, it is the aim of this work to work out a improved method for the utilization of wind-power by analysing the characteristics of horizontal axis wind turbine and its simulation system. The simulation system of horizontal axis wind turbine can accelerate the practical use of wind energy in rural area.

1.3   THE SCOPE OF THE THESIS

This thesis presents a improved method for the utilization of wind-power by analysing the characteristics of horizontal axis wind turbine and its simulation system. In this simulation system, an electric motor is used whose performance is closed to the wind turbine. With these simulated system , either a wind pump or an electricity generator can be coupled.

In chapter one, a short historical background of wind turbines is given. The aim of the thesis, the scope of the thesis, and the review of the existing literature are also presented in this chapter.

Chapter two deals with the momentum theory and the blade element theory together with the strip theory, tip and hub losses, lift and drag forces on the airfoil-shaped blades.

In chapter three, different characteristics of three-bladed and six-bladed horizontal axis wind turbine are determined by experimental method. The experiments are to be carried out in the project laboratory with the wind tunnel. The air flows through the wind tunnel with high velocity and this high velocity air is controlled to rotate the wind turbine. The wind turbine is tested at different air velocities to determine coefficient of power (C_p), torque coefficient (C_T), and C_p-λ, C_T-λ characteristics. Finally, the characteristics of three-bladed wind turbine are compared to the characteristics of six-bladed wind turbine.

In chapter four, the load characteristics of an electric motor is determined. Then the performance characteristics of this electric motor is compared to the performance characteristics of the wind turbine and made close to the wind turbine characteristics. With these simulated system either a wind pump or an electricity generator can be coupled.

Chapter five deals with the actual results obtained from the experiments on the horizontal axis wind turbine and its simulation system. The discussion on these results are also illustrated in this chapter.

In chapter six , conclusions and recommendations are presented.

1.4 REVIEW OF EXISTING LITERATURES

The horizontal axis wind turbine extracts energy from the driving air and converts it into a mechanical power in contrast to a propeller which adds energy into the air from another energy source. Because of the similarity of the wind turbine and the propeller, it is possible to use the same theoretical development for the performance analysis. The propeller theory was based on two different independent approaches. One is the momentum theory approach and the other is the blade element theory approach.

The first description of the axial momentum theory was given by Rankine [3] in 1865 and was improved later by Froude [4]. The basis of the theory is the determination of the forces acting on the rotor which produces the motion of the fluid. It also predicts the ideal efficiency of the rotor. Later on Betz [5] included the rotational wake effects in the theory.

The application limit of the momentum theory is the state where reverse flow begins to occur downstream of the rotor. The operating states of a wind turbine can be classified theoretically into four categories namely, the propeller state, the windmill state, the turbulent wake state, and the vortex ring state. These states can occur simultaneously at different positions of a blade. In the helicopter analysis, several experimental studies have been made on the vortex ring state and on the turbulent wake state. Lock [6, 7] conducted wind tunnel tests using two model rotors and Glauert [8] defined a characteristic curve utilizing the data of Lock. While Gessow [9] conducted a flight test of a helicopter to obtain a similar characteristic curve, and

16

its approximate formula has given by Johnson [10]. Wilson [11] has suggested linear algebraic expressions for the local thrust at high tip speed ratios where a wind turbine may operate in the vortex ring state. There is very little published literature on the performance of a wind turbine operating in the turbulent wake state. Yamane [12] has introduced a performance prediction method for windmill in the turbulent wake state utilizing the empirical characteristic curve of Gessow or of Lock and Glauert in combination with blade element theory. Recently, Anderson [13] has published the results of a vortex-wake analysis of a horizontal axis wind turbine and he has compared his results with those obtained from the modified blade element theory. He suggests that unless information is required about the wake, it is satisfactory to use the blade element theory with a suitable model for tip loss. The vortex-wake analysis has advantages over modified blade element theory is that it provides information on the radial flow and the axial velocity deficit in the wake. The main disadvantage of the vortex-wake analysis is the computational time necessary to obtain a solution. Viterna [14] has suggested an improve method to calculate the aerodynamic performance of a horizontal axis wind turbine at tip speed ratios where aerodynamic stall can occur as the blade experiences high angles of attack.

Walker [15] has developed a method to determine the blade shapes for maximum power. According to his method, the blade chord and twist are continuously varied at each radial station until the elemental power coefficient has been maximized. This is obtained when every radial element of the blade is operating at the airfoil's maximum lift to drag ratio. This results in the lift coefficient and angle of attack being identical at each radial element. Anderson [16] has compared near-optimum and optimum blade shapes for turbines operating at both constant tip speed ratio and constant rotational speed. Shepherd [17] has suggested a simplified method for design and performance analysis of a horizontal axis wind turbine which can be

carried out on a hand-held calculator by elimination of iteration processes. It is based on the use of the ideal and optimized analysis to determine the blade geometry. It requires only fixed values of the axial induction factors and corresponding optimized rotational induction factors.

Jansen [18] has worked on the theories that from the basis for calculation of the design and the behaviour of a windmill. A modification of the Prandtl model of tip losses is derived. This modification takes the relatively heavy loading of the windmill rotor into account. It is argumented that, in contrast with propeller design, a maximum energy extraction is reached by enlarging the chords of the blades near the tips. Selection, design and construction of several rotors and of a test unit are described in his report. He has concluded that with simple materials high power coefficients are possible.

Large horizontal axis wind turbines must be designed for structural efficiency and reliability together with minimum maintenance and weight in order to produce energy at a competitive cost. Major factors which dictate structural weight are the vibratory loads which act on the rotor and the tower. These unsteady loads may be aerodynamic, gravitational, or inertial in origin. For very large wind turbines vibratory stresses caused by dynamic loads will probably be the governing design consideration [19]. An analysis was made by Wilcox [20] and his co-workers together with Von Karman on the 1250 kilowatt Smith-Putnam wind power system, in an effort to minimize vibratory loads on the tower. Spera [21] analyzed the vibratory loads and stresses in the hingeless and teetered rotors for the NSF-NASA MOD-O wind power system. He concluded that the teetered rotor had substantial advantages over the hingeless rotor with respect to shank, stresses, fatigue life, and tower loading. The hingeless rotor analyzed does not appear to be structurally stable

during overloads. Therefore, until adequate reliability of associated automatic controls has been established, a teetering rotor will probably be required in order to achieve a long service life in a wind turbine which operates unattended.

Glasgow [22] carried out tests on MOD-O wind turbines considering downwind and upwind wind directions. As a result of the tests, it is shown that while mean flatwise bending moments were unaffected by the placement of the rotor, cycle flatwise bending tended to increase with wind speed for the downwind rotor while remaining somewhat uniform with wind speed for the upwind rotor, reflecting the effects of increased flow disturbances for a downwind rotor. Nacelle yaw moments are higher for the upwind rotor but do not indicate significant design problems for either configuration. Linscott [23] has analyzed and measured the natural frequencies of MOD-O wind turbines. Good agreement between calculated and measured loads was obtained in an analysis that included only two blade dynamic modes, first flap and first enplane, and a blade quasi-steady mode.

Milborrow [24] worked out in the field of rotor performance, blade loading, stresses and size limits of horizontal axis wind turbines. In order to identify the variables which influence performance and blade loading, simplified methods of analysis have been developed and used to illustrate the process of rotor design. The tip speed ratio and number of blades are shown to have a strong influence on stress levels and the analysis indicates why a preference for two blades has emerged for large machines. It is also known that the maximum stresses do not necessarily occur at the blade roots and assessments are made of the relative magnitude of stresses due to the principal load sources in both edgewise and flapwise directions. Spera and Janetzke [25] studied the effects of rotor location, coning and tilt on critical loads in large wind turbine. These large horizontal axis rotor configurations were analyzed to determine

the effects on dynamic loads of upwind and downwind rotor locations, coned and radial blade positions, and tilted and horizontal rotor axis positions. Loads were calculated for a range wind velocities at three locations in the structure: the blade shank, the hub shaft, and the yaw drive. Blade axis coning and rotor axis tilt were found to have little effects on loads. However, locating the rotor upwind of the tower significantly reduced loads at all locations analyzed.

Powells [26, 27] investigated the effects of tower shadow on a downwind two-bladed horizontal axis wind turbine. A rotor aeroelastic simulation is used to predict the blade response to tower shadow, and subsequently to estimate increased blade fatigue damage. He suggested to reduce the effect of tower shadow by making the tower more aerodynamically smooth, thereby reducing the flow disturbance. However, because of changes in wind direction, it is necessary to have an aerodynamic tower fairing which is free to move in yaw with the turbine nacelle. The use of an aerodynamically streamlined fairing has been shown to have a beneficial effect on the strain and cone angle variations in the blades of a hinged-blade downwind horizontal axis wind turbine. The reduction of about one-third in amplitude in each case indicates that the use of such a fairing should have a significant effect in extending the fatigue life of downwind horizontal axis wind turbines in general. For rigid or teetered blades the reductions in strain variation should be even more significant. Since an effective fairing has been easily and cheaply built, and since it encounters a far easier regime than the blades of the machine, it follows that this may well be a worthwhile addition for small and medium size downwind machines. The reduction in the noise levels observed would help to make such machines more environmentally acceptable as well.

Wentz [28] has conducted studies to determine the possibilities of aileron or spoiler controls as alternatives to pitch control for large horizontal axis wind turbines. The NASA MOD-O machine was used as the basis for this study. Results of the study show that either aileron or spoilers can provide control necessary to limit turbine power in high wind conditions. An aileron system is recommended to provide self-starting and added power at low wind speed conditions and provides overs peed protection at hurricane wind speed.

CHAPTER-2

STUDY OF THE EXISTING THEORIES OF WIND TURBINE

The main perpose of a wind turbine is to extract energy from the air flow and convert it into mechanical energy which later may be transformed into other forms of energy. The performance calculation of wind turbines are mostly based upon a steady flow, in which the influence of the turbulence of the atmospheric boundary layer is neglected. For determining the performance characteristics of the wind turbine, most existing theoretical models are based on the combination of momentum theory and blade element theory. This combined theory is known as modified blade element theory or strip theory. It has been assumed that the strip theory approaches will be adequate for wind machines performance analysis. Based on this analysis, the wind turbine can be replaced by an electric motor whose performance can be made close to the wind turbine. For determining the performance of electric D.C Motor in these simulated system, it must be need to find the speed of motor at different voltage and current.

2.1   AXIAL MOMENTUM THEORY

The axial momentum theory was presented by Rankine in 1865 and later modified by Froude [9]. The theory determines the forces, acting on the rotor to create motion of the fluid. The theory is useful to predict the ideal efficiency of a wind turbine. For the maximum possible output of a wind turbine the assumptions underlying the axial momentum theory are:

1.   The fluid is inviscid and incompressible.

2.   Infinite number of blades.

3.   Flow is entirely axial with no rotational motion.

4.   Thrust loading is uniform over the disc.

5.   The flow is homogeneous.

6.   Static pressure for ahead and for behind the rotor are equal to the undisturbed ambient static pressure.

Considering the control volume ABCD in Figure 2.1.1, where the up-stream and down-stream control volume planes are infinitely far removed from the turbine plane, the conservation of mass may be expressed as:

$$\rho \, A_1 \, V_\infty = \rho \, A \, U = \rho \, A_2 \, V \qquad (2.1.1)$$

Where,

   V_∞= undisturbed wind velocity

   U = wind velocity through the rotor

   A = turbine disc area where velocity of wind is U.
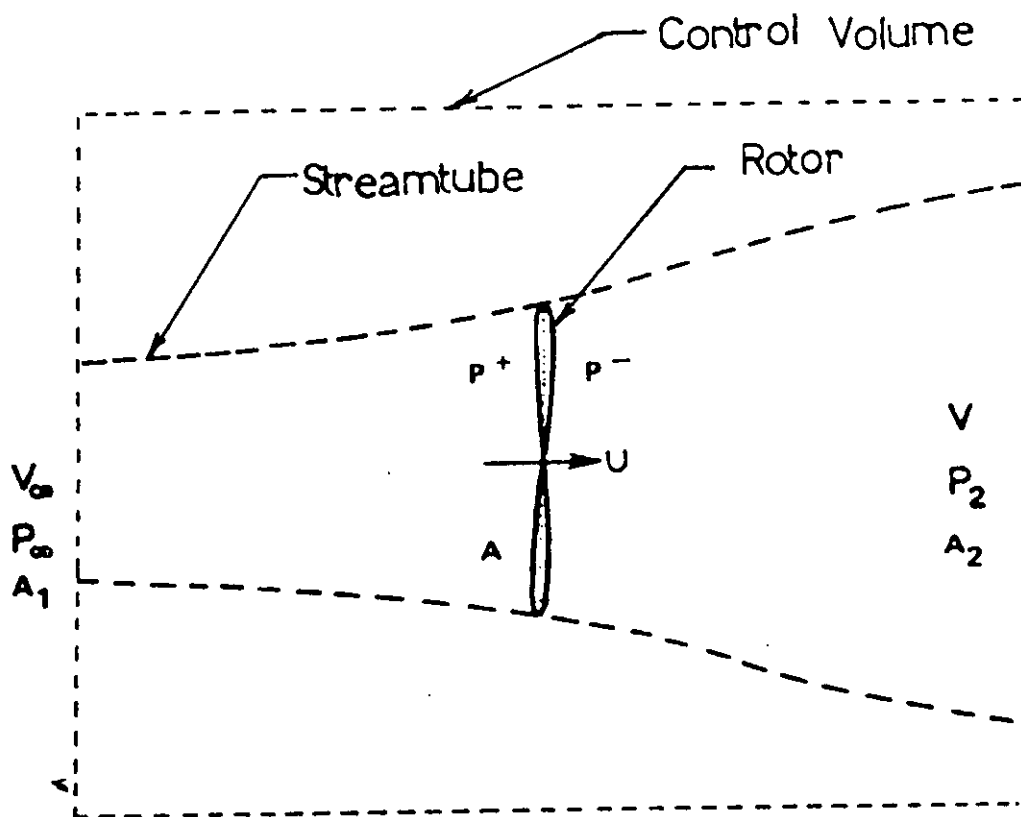
Figure 2.1.1 : Control Volume of a Wind Turbine

ρ

A_1 = cross-sectional area of incoming wind.

A_2 = wake cross-sectional area.

The thrust force Q, on the rotor is given by the change of momentum of the flow:

$$Q = \dot{m} \, (V_\infty - V) = \rho \, A_1 \, V_\infty^2 - \rho \, A_2 \, V^2 \qquad (2.1.2)$$

So from equation (2.1.1) and (2.1.2) we get,

$$Q = \rho \, A \, U \, (V_\infty - V) \qquad (2.1.3)$$

The thrust on the rotor can also be expressed from the pressure difference over the rotor area:

$$Q = A \, (P^+ - P^-) \qquad (2.1.4)$$

Where,

P^+ = pressure immediately in front of the rotor

P^- = pressure immediately behind the rotor

Now applying Bernoulli's equation:

for upstream of the rotor:
$$P_\infty + \frac{1}{2} \rho \, V_\infty^2 = P^+ + \frac{1}{2} \rho \, U^2 \qquad (2.1.5)$$

for downstream of the rotor:
$$P_\infty + \frac{1}{2} \rho \, V^2 = P^- + \frac{1}{2} \rho \, U^2 \qquad (2.1.6)$$

Substracting equation (2.1.6) from equation (2.1.5), we get

$$P^+ - P^- = \frac{1}{2} \rho (V_\infty^2 - V^2)$$ (2.1.7)

and the expression for the thrust from equation (2.1.4) becomes

$$Q = \frac{1}{2} \rho A (V_\infty^2 - V^2)$$ (2.1.8)

Equating the equation (2.1.8) with equation (2.1.3)

$$Q = \frac{1}{2} \rho A (V_\infty^2 - V^2) = \rho A U (V_\infty - V)$$

$$\therefore U = \frac{V_\infty + V}{2}$$ (2.1.9)

Here, the velocity of the wind at the rotor may be calculated by simply measuring the velocity of upstream, V_∞ and downstream V of the flow with Anemometer.

So the thrust force Q, on the rotor is $Q = \rho A U (V_\infty - V)$ which can be calculated by knowing U and the thrust Q is depend on the velocity of the wind.

Now the velocity at the rotor U is often defined in terms of an axial interference factor f, as

$$U = V_\infty (1 - f)$$

So, $$U = \frac{V_\infty + V}{2} = V_\infty (1 - f)$$

$$V = V_\infty \ (1 - 2f) \qquad\qquad (2.1.10)$$

So, the change in kinetic energy of the mass flowing through the rotor area is the power absorbed by the rotor:

$$P = \dot{m} \ \Delta KE = \frac{1}{2} \rho \ A \ U \ (V_\alpha^2 - V^2) \qquad\qquad (2.1.11)$$

or,
$$P = \frac{1}{2} \rho \ A \ V_\infty \ (1-f) \left[V_\infty^2 - V_\infty^2 \ (1-2f)^2 \right]$$

$$\therefore P = 2 \ A \ V_\infty^2 \ f \ (1-f)^2 \qquad\qquad (2.1.12)$$

Maximum power occurs when, $\dfrac{dP}{df} = 0$

Therefore,
$$\frac{dP}{df} = 2 \ \rho \ A \ V_\infty^3 \ (1 - 4f + 3f^2) = 0$$

which leads to an optimum interference factor,

$$f = 1/3$$

$$\therefore P_{max} = 2 \ \rho \ A \ V_\infty^3 \ \frac{1}{3} \left(1 - \frac{1}{3}\right)^2$$

$$\therefore P_{max} = \frac{16}{27} \cdot \left(\frac{1}{2} \rho \ A \ V_\infty^2 \right) \qquad\qquad (2.1.13)$$

27

The factor $\dfrac{16}{27}$ is called the Betz-Coefficient and represents the maximum fraction which an ideal rotor can extract from the flow.

Now by apply torque on the rotor, the rotor power P, can be measured. If T is the torque applied to the shaft and N is the revolution/min. of the shaft. Then,

$$\omega = \frac{2\pi N}{60}$$

So power of the rotor, $\qquad P = T\omega$

So, power coefficient $\qquad C_p = \dfrac{P}{\dfrac{1}{2}\rho A V_\infty^3}$ $\qquad\qquad$ (2.1.14)

where $\qquad \dfrac{1}{2}\rho A V_\infty^3$ is the total flow energy.

Again, if R is the radius of the blade that the tip speed ratio, $\lambda = \dfrac{\omega R}{V_\infty}$ $\qquad$ (2.1.15)

So, Torque coefficient, $\qquad C_T = \dfrac{T}{\dfrac{1}{2}\rho A V_\infty^2 R}$ $\qquad\qquad$ (2.1.16)

Thrust coefficient, $\qquad C_Q = \dfrac{Q}{\dfrac{1}{2}\rho A V_\infty^2}$ $\qquad\qquad$ (2.1.17)

2.2 EFFECT OF WAKE ROTATION ON MOMENTUM THEORY

Considering this effect the assumption is made that at the upstream of the rotor the flow is entirely axial and the downstream flow rotates with an angular velocity ω' but remains irrotational. This angular velocity is considered to be small in comparison to the angular velocity ω of the wind turbine. This assumption maintains the approximation of axial momentum theory that the pressure in the wake is equal to the free stream pressure.

The wake rotation is opposite in direction of the rotor and represents an additional loss of kinetic energy for the wind rotor. Power is equal to the product of the torque T acting on the rotor and the angular velocity ω of the rotor. In order to obtain the maximum power it is necessary to have a high angular velocity and low torque because high torque will result in large wake rotational energy. The angular velocity ω' of the wake and the angular velocity ω of the rotor are related by an angular interference factor f';

$$f' = \frac{\omega'}{2\omega} \qquad (2.2.1)$$

The annular ring through which a blade element will pass is illustrated in Figure. 2.2.3

Using the relation for momentum flux through the ring the axial thrust force dQ can be expressed as

$$dQ = dm \, (V_\infty - V) = \rho \, dA \, U \, (V_\infty - V)$$
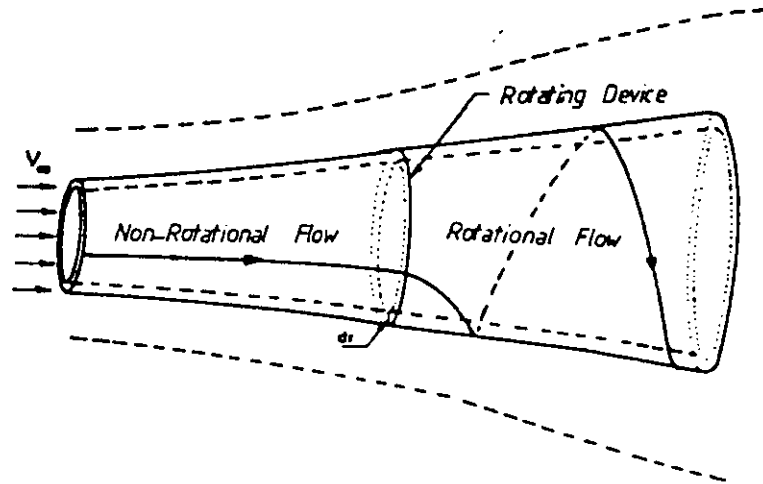
Figure 2.2.2 : Streamtube Model Showing the Rotation of Wake.
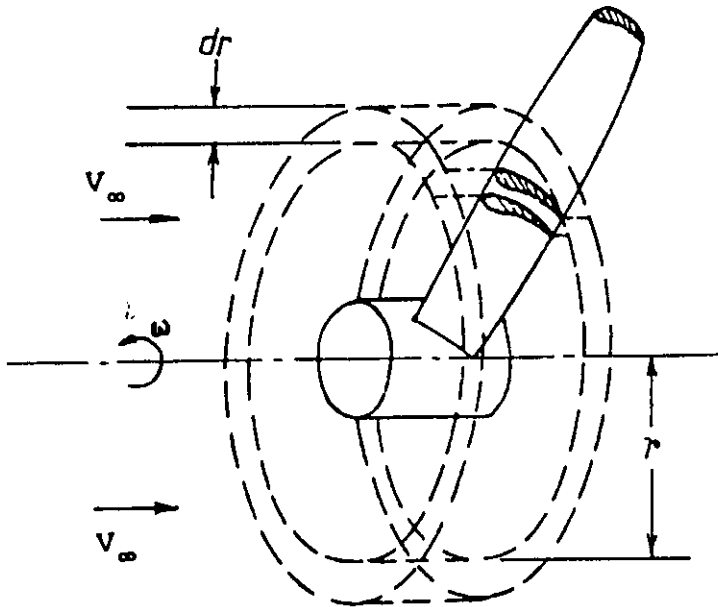
Figure 2.2.3 : Blade Element Annular Ring.

$$dQ = 4\pi \, r \, \rho \, V_\infty^2 \, f \, (1-f) \, dr \qquad\qquad (2.2.2)$$

By putting $u = V_\infty \, (1 - f)$, $V = V_\infty \, (1 - 2f)$ and expressing the area of the annular ring dA as

$$dA = 2\pi \, r \, dr \qquad\qquad (2.2.3)$$

The thrust force may also be calculated from the pressure difference over the blades by applying Bernoulli's equation. Since the relative angular velocity changes from ω to $(\omega + \omega')$, while the axial components of the velocity remain unchanged, Bernoulli's equation gives

$$P^+ - P^- = \frac{1}{2} \, \rho \, (\omega + \omega')^2 \, r^2 - \frac{1}{2} \, \rho \, \omega^2 \, r^2$$

or,
$$P^+ - P^- = \rho \, (\omega + \frac{1}{2} \, \omega') \, \omega' \, r^2$$

The resulting thrust on the annular element is given by,

$$dQ = (P^+ - P^-) \, dA$$

or,
$$dQ = \rho \, (\omega + \frac{1}{2} \, \omega') \, \omega' \, r^2 \, 2\pi \, r \, d \, r$$

Inserting equation (2.2.1)

$$dQ = 4f' \, (1 + f') \, \frac{1}{2} \, \rho \, \omega^2 \, r^2 \, 2\pi \, r \, d \, r \qquad\qquad (2.2.4)$$

Balancing equation (2.2.4) and equation (2.2.2), leads to the expression

$$\frac{f(1-f)}{f'(1+f')} = \frac{\omega^2 r^2}{V_\infty^2} = \lambda_r^2 \qquad (2.2.5)$$

Where λ_r is known as the local tip speed ratio which is given by

$$\lambda_r = \frac{r\omega}{V_\infty} \qquad (2.2.6)$$

To derive an expression for the torque acting on the rotor the change in angular momentum flux dT through the annular ring is considered.

$$dT = dm \ V_t \ r$$

or, $\quad dT = \omega' r \rho \ dA \ U \ r$

Where V_t is the wake tangential velocity.

So, the expression for the torque acting on the annular ring is given by

$$dT = 4\pi \ r^3 \ \rho \ V_\infty \ (1-f) \ f' \omega \ d \ r \qquad (2.2.7)$$

The generated power through the annular ring is equal to $dp = \omega dT$, so the total power becomes

$$P = \int_O^R \omega \ d \ T \qquad (2.2.8)$$

Introducing the tip speed ratio λ as

$$\lambda = \frac{R\omega}{V_\infty} \qquad (2.29)$$

Equation for total power from equation (2.2.7) and equation (2.2.8) becomes

$$P = \int_O^R 4\pi\, r^3\, \rho\, V_\infty\, (1-f)\, f'\, \omega^2\, d\,r$$

This can be written as

$$P = \frac{1}{2}\rho\, A\, V_\infty^3\, \frac{8}{\lambda^2} \int_o^\lambda f'\, (1-f)\, \lambda_r^3\, d\,\lambda_r \qquad (2.2.10)$$

Where A is the turbine swept area which is given by $A = \pi\, R^2$.

The power coefficient is defined as

$$C_P = \frac{P}{\frac{1}{2}\rho\, A\, V_\infty^3}$$

Inserting equation (2.2.10), power coefficient can be written as

$$C_P = \frac{8}{\lambda^2} \int_o^\lambda f'\, (1-f)\, \lambda_r^3\, d\,\lambda_r \qquad (2.2.11)$$

Rearranging equation (2.2.5)

$$f' = \frac{-1}{2} + \frac{1}{2}\sqrt{1 + \frac{4}{\lambda_r^2} f\,(1-f)} \qquad (2.2.12)$$

Substituting this value is equation (2.2.1) and taking the derivative equal to zero, the relation between λ_r and f for maximum power becomes

33

$$\lambda_r = \frac{(1-f)(4f-1)^2}{(1-3f)} \qquad (2.2.13)$$

Introducing equation (2.2.13) in the equation (2.2.5), the relationship between f and f' becomes:

$$f' = \frac{1-3f}{4f-1} \qquad (2.2.14)$$

This relation is used for design purposes.

2.3 LIFT AND DRAG FORCES ON THE AIRFOIL-SHAPED BLADES

Power coefficient of the wind turbine is affected by C_D and C_L values of the airfoil sections. For a fast running load a high design tip speed ratio will be selected and airfoils with a low C_D/C_L ratio will be preferred. But for wind turbines having lower design tip speed ratios the use of more blades compensates the power loss due to drag. so airfoils having higher C_D/C_L ratio are selected to reduce the manufacturing cost. For the design and performance calculations of the wind turbines two-dimensional airfoil data are to be used in terms of lift and drag coefficients. The available data are normally limited to a range of angles of attack upto maximum lift and the behaviour above this is not well known. The data are suitable for big wind turbines covering Reynolds number 3×10^6 to 9×10^6. For smaller wind turbines when the Reynolds number is less than 1×10^6 reliable airfoil data are rarely available. Surface roughness effects on airfoil data are not very well known. For different types of airfoils the sensitivity for surface roughness are also different. Using airfoil data for NACA standard roughness in wind turbine performance

calculations results in losses in peak performance of the order of 10 -15% in comparison with usual airfoil data for a smooth surface.

When a airfoil placed in a uniform flow, a force is exerted on the airfoils, of which the direction is generally not parallel to the direction of the undisturbed flow. One part of the force, in the direction perpendicular of the undisturbed flow is called the lift and the other part of the force, in the direction of the undisturbed flow is called the drag. For a smooth airfoil these force are shown in Figure 2.3.1.

In physical terms the force on an airfoil is caused by the changes in the flow velocities around the airfoil. On the upper side of the airfoil, the velocities are higher than on the bottom side. The result is that the pressure on the upper side is lower than the pressure on the bottom side, hence the creation of the force F.

In describing the lift and drag properties of different airfoils, reference is usually being made to the dimensionless lift and drag coefficients which are defined as follows:

Lift coefficient, $\qquad C_L = \dfrac{L}{\dfrac{1}{2}\rho V_\infty^2 A}$

Drag coefficient, $\qquad C_D = \dfrac{D}{\dfrac{1}{2}\rho V_\infty^2 A}$

With ρ = density of air

V_∞ = undisturbed wind speed (m/s)

A = projected blade area (chord*length) (m^2)

These dimensionless lift and drag coefficients are measured in wind tunnels for a range of angles of attack α. This is the angle between the direction of the undisturbed wind speed and a reference line of the airfoil. For a curved plate the reference line is simply the line connecting leading and trailing edge, while for an airfoil it is the line connecting the trailing edge with the center of the smallest radius of curvature at the leading edge.

The values of power coefficient C_p and drag coefficient C_D of a given airfoil very with the wind speed or, better, with the Reynolds number Re. The Reynolds number is a vital dimensionless parameter in fluid dynamics and is defined as $Re = Vc/v$,

with, V = the undisturbed with speed

C = the characteristic length of the body (here the chord of the airfoil)

and v = the kinematic viscosity of the fluid (for air at 20°C the value of V is

$15*10^{-6} \, m^2/s$)

If the influence of Reynolds number can be neglect due to a second-order effect, then the C_L-α and C_L - C_D curves for the proper value of Re can be drawn as follows: (Figure 2.3.2)

The tangent to the C_L - C_D curve drawn from the origin indicates the angle of attack with the minimum C_L/C_D ratio. This ratio of strongly determines the maximum power coefficients that can be reached particularly at high tip speed ratios.
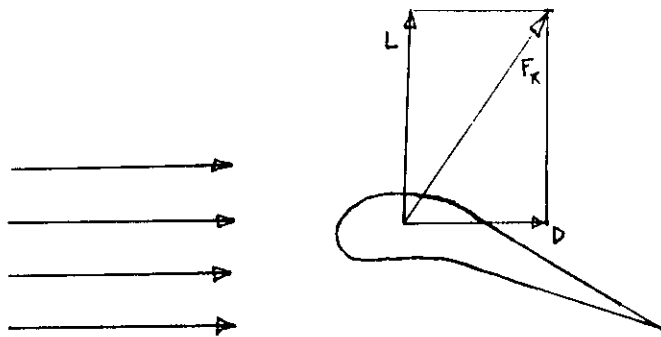
Figure. 2.3.1 : Lift and Drag for a smooth airfoil- shaped blade.
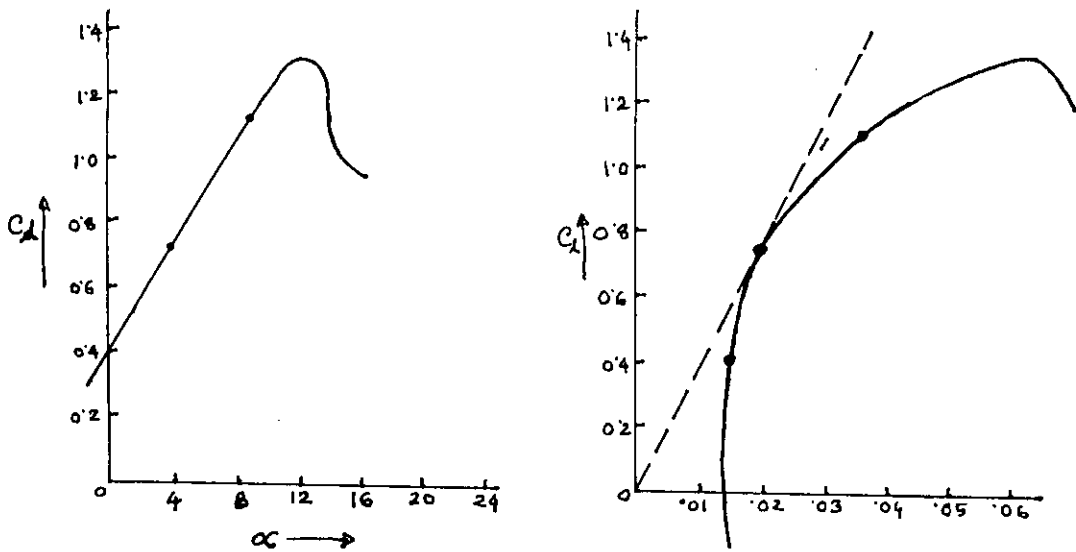
Figure. 2.3.2 : THE Lift and Drag coefficient of a given airfoil.

37

The values of α and C_L at minimum C_L/C_D ratio are important parameters in the design process. The values for some airfoils are given in the table below (Figure 2.3.3)

	C_L/C_D	α	C_L
Flat plate	0.1	5°	0.8
Curved plate (10 x curvature)	0.02	3°	1.25
Curved plate with tube on convex side	0.03	4°	1.1
Curved plate with tube on convex side	0.2	14°	1.25
Airfoil NACA 4412	0.01	4°	0.8

Figure. 2.3.3: Typical values of the drag-lift ratio C_L/C_D and α and C_L for a number of airfoils.

The role of the lift and drag forces in the behaviour of a blade of a horizontal-axis wind rotor can be determined by examined the wind speeds on a cross section of the blade looking from the tip to the roof of the blade.

2.4 BLADE ELEMENT THEORY

With the blade element theory the forces acting on a differential element of the blade may be calculated. Then integration is carried out over the length of the blade to determine the performance of the entire rotor. The assumptions underlying the blade element theory are:

1. There is no interference between adjacant blade elements along each blade.

2. The forces acting on a blade element are solely due to the lift and drag characteristics of the sectional profile of the element.

3. The pressure in the far wake is equal to the free stream pressure.

The aerodynamic force components acting on the blade element are the lift force dL perpendicular to the resulting velocity vector and the drag force dD acting in the direction of the resulting velocity vector. The following expressions for the sectional lift and drag forces may be introduced:

$$dL = C_L \frac{1}{2} \rho V_r^2 C d r \qquad (2.4.1)$$

$$dD = C_D \frac{1}{2} \rho V_r C d r \qquad (2.4.2)$$

With C is the chord of the blade.

The thrust and torque expressed by the blade element are

$$dQ = dL \cos\phi + dD \sin\phi \qquad (2.4.3)$$

$$dT = (dL \sin\phi + dD \cos\phi) \, r \qquad (2.4.4]$$

Assuming that the rotor has B blades, the expressions for the thrust and torque become

$$dQ = BC \frac{1}{2} \rho \, V_r^2 \, (C_L \cos\phi + C_D \sin\phi) \, d\,r$$

$$\text{or,} \quad dQ = BC \frac{1}{2} \rho \, V_r^2 \, C_L \cos\phi \, (1 + \frac{C_D \tan\phi}{C_L}) \, d\,r \qquad (2.4.5)$$

and

$$dT = BC \frac{1}{2} \rho \, V_r^2 \, (C_L \cos\phi + C_D \sin\phi) \, r \, d\,r$$

$$\text{or,} \quad dT = BC \frac{1}{2} \rho \, V_r^2 \, C_L \sin\phi \, (1 - \frac{C_D}{C_L} \frac{1}{\tan\phi}) \, r \, d\,r \qquad (2.4.6)$$

According to the Figure 2.4.1, the expression for related velocity V_r can be written as

$$V_r = \frac{(1-f) \, V_\infty}{\sin\phi} = \frac{(1-f') \, \omega \, r}{\cos\phi} \qquad (2.4.7)$$

Introducing the following trigonometric relations based on Figure 2.4.1,

$$\tan\phi = \frac{(1-f) \, V_\infty}{(1-f') \, \omega \, r} = \frac{1-f}{1+f'} \frac{1}{\lambda_r}$$

and $$\qquad \beta_T = \phi - \alpha$$

40

and the local solidity ratio σ as

$$\sigma = \frac{BC}{2\pi\, r}$$

The equations of the blade element theory become

$$dQ = (1-f)^2\, \frac{\sigma\, C_L\, \cos\phi}{\sin^2\phi}\left(1 + \frac{C_D}{C_L}\, \tan\phi\right)\frac{1}{2}\, \rho\, V_\alpha^2\, 2\pi\, r\, d\, r \quad (2.4.8)$$

$$dT = (1-f')\, \frac{\sigma\, C_L\, \sin\phi}{\cos^2\phi}\left(1 - \frac{C_D}{C_L}\, \frac{1}{\tan\phi}\right)\frac{1}{2}\, \rho\, \omega^2\, r^3\, 2\pi\, r\, d\, r \quad (2.4.9)$$

2.5   STRIP THEORY

From the axial momentum and blade element theories a series of relationships can be developed to determine the performance of a wind turbine.

From momentum theory, it can be seen that the equation of dT_m and dQ_m is

$$dT_m = 4\pi\, r^3\, \rho\, V_\infty\, (1-f)\, f'\, \omega\, d\, r \qquad\qquad (2.5.1)$$

$$dQ_m = 4\pi\, r^3\, \rho\, V_{2\infty}\, (1-f)\, d\, r \qquad\qquad (2.5.2)$$

From blade element theory it can be seen that the equation of dT_m and dQ_m is:

$$dT_b = (1+f')\, \frac{\sigma\, C_L\, \sin\phi}{\cos^2\phi}\left(1 - \frac{C_D}{C_L}\, \frac{1}{\tan\phi}\right)\frac{1}{2}\, \rho\, \omega^2\, r^3\, 2\pi\, r\, d\, r \quad (2.5.3)$$

41

$$dQ_b = (1+f)^2 \frac{\sigma\, C_L \cos\phi}{\sin^2\phi}\left(1 + \frac{C_D}{C_L}\tan\phi\right)\frac{1}{2}\,\rho\, V_\infty^2\, 2\pi\, r\, d\, r \quad (2.5.4)$$

Now equating the equation 2.5.2 and 2.5.4 we get,

$$dQ_m = dT_m$$

or,
$$\frac{f}{1-f} = \frac{\sigma\, C_L \cos\phi}{4\sin^2\phi}\left(1 + \frac{C_D}{C_L}\tan\phi\right) \qquad (2.5.5)$$

$$dQ_m = dT_b$$

or,
$$\frac{f'}{1-f'} = \frac{\sigma\, C_L}{4\cos\phi}\left(1 - \frac{C_D}{C_L}\frac{1}{\tan\phi}\right) \qquad (2.5.6)$$

Equations (2.5.5) and equations (2.5.6) which determine the axial and angular interferance factors contain drag terms. Omitting the drag terms the induction factors f and f' may be calculated with the following equations:

$$\frac{f}{1-f} = \frac{\sigma\, C_L \cos\phi}{4\sin^2\phi} \qquad (2.5.7)$$

$$\frac{f'}{1+f'} = \frac{\sigma\, C_L}{4\cos\phi} \qquad (2.5.8)$$

Considering equations (2.5.6) and equations (2.5.4) elemental thrust can be written as

$$dQ = 4f\,(1-f)\left(1 + \frac{C_D}{C_L}\tan\phi\right)\frac{1}{2}\,\rho\, V_\infty^2\, 2\pi\, r\, d\, r$$

42

From equation (2.5.8) and (2.5.3), elemental torque can be obtained as,

$$dT = 4f' \; (1-f) \left(1 - \frac{C_D}{C_L} \frac{1}{\tan\phi}\right) \frac{1}{2} \rho \; V_\infty \omega \; 2\pi \; r^3 \; d\,r$$

Elemental power is given by

$$dP \;=\; dT \; \omega$$

or,

$$dP = 4f' \; (1-f) \left(1 - \frac{C_D}{C_L} \frac{1}{\tan\phi}\right) \frac{1}{2} \rho \; V_\infty \; \omega \; 2\pi \; r^3 \; d\,r$$

Introducing the local tip speed ratio λ_r with:

$$\lambda_r = \frac{\omega r}{V_\infty}$$

Equations of total thrust, torque and power become

$$T = \frac{1}{2} \rho \; A \; V_\infty^2 \; R \frac{8}{\lambda^3} \int_o^\lambda f' \; (1-f) \left(1 - \frac{C_D}{C_L} \frac{1}{\tan\phi}\right) \lambda_r^3 \; d\,\lambda_r$$

$$Q = \frac{1}{2} \rho \; A \; V_\infty^2 \frac{8}{\lambda^2} \int_o^\lambda f \; (1-f) \left(1 + \frac{C_D}{C_L} \tan\phi\right) \lambda_r \; d\,\lambda_r$$

and

$$T = \frac{1}{2} \rho \; A \; V_\infty^3 \frac{8}{\lambda^2} \int_o^\lambda a' \; (1-a) \left(1 - \frac{C_D}{C_L} \frac{1}{\tan\phi}\right) \lambda_r^3 \; d\,\lambda_r$$

These equations are valid only for a wind turbine having infinite number of blades.

43

2.6 TIP AND HUB LOSSES

In the proceeding sections the rotor was assumed to be possessing an infinite number of blades with an infinitely small chord. In reality, however, the number of blades is finite. According to the theory discussed previously, the wind imparts a rotation to the rotor, thus dissipating some of its kinetic energy or velocity and creating a pressure difference between one side of the blade and the other. At tip and hub, however, this pressure difference leads to secondary flow effects. The flow becomes three-dimensional and tries to equalize the pressure difference as shown in Fig. 2.6.a.

This effect is more pronounced as one approaches the tip. It results in a reduction of the torque on the rotor and thus in a reduction of the power output.

Several alternative models to take this loss into account exist. The method suggested by Prandtl will be used here. The idea in Prandtl's method is to replace the system of vortices at the tip with a series of parallel planes for which the flow is more easily calculated.

It should however be remembered that this approximation was developed for a lightly loaded propeller under optimum conditions which may differ somewhat from the conditions of a wind turbine.

The correction factor suggested by Prandtl is

$$F_{tip} = \frac{2}{\pi} \text{ arc } \cos e^{-a}$$

44

where
$$a = \frac{B}{2} \frac{R-r}{R \sin\phi}$$

It may also be applied for the hub region and "a" is then defined as

$$"a" = \frac{B}{2} \frac{r - r_{Hub}}{r_{Hub} \sin\phi}$$

Hence, a correction factor F_f for total losses is applied as,

$$F_f = F_{tip} \, r_{Hub}$$

The loss factor F_f may be introduced in several ways for the rotor performance calculations. In the method adopted by Wilson and Lissaman, the induction factors f and f' are multiplied with F, and thus the axial and tangential velocities in the rotor plane as seen by the blades are modified. It is further assumed that these corrections only involve the momentum formulas.

Thus the thrust and torque from momentum theory become

$$dQ = 4\pi \, r \, \rho \, V_\infty^2 \, f \, F \, (1 - fF) \, dr \qquad (2.6.2)$$

$$dT = 4\pi \, r^3 \, \rho \, V_\infty f' \, F \, (1 - fF) \, \omega \, dr \qquad (2.6.3)$$

The results of the blade element theory remain unchanged.

$$dQ = (1-f)^2 \, \frac{\sigma \, C_L \, \cos\phi}{\sin^2\phi} \left(1 + \frac{C_D}{C_L} \tan\phi \right) \frac{1}{2} \rho \, V_\infty^2 \, 2\pi \, r \, dr \quad (2.6.4)$$

and

$$dT = (1+f')^2 \, \frac{\sigma \, C_L \, \tan\phi}{\cos\phi} \left(1 - \frac{C_D}{C_L} \frac{1}{\tan\phi} \right) \frac{1}{2} \rho \, V_\infty^2 \, 2\pi \, r \, dr \quad (2.6.5)$$

45

Equation (2.6.4) can also be written as

$$dT = (1-f)^2 \frac{\sigma C_L}{\sin\phi} \left(1 - \frac{C_D}{C_L} \frac{1}{\tan\phi}\right) \frac{1}{2} \rho V_\infty^2 \, 2\pi \, r^2 \, d\,r \qquad (2.6.6)$$

Balancing the equation (2.6.2) with (2.6.4) one finds

$$fF = (1 - fF)^2 = \frac{\sigma C_L \cos\phi \, (1-f)^2}{4\sin^2\phi} \left(1 - \frac{C_D}{C_L} \tan\phi\right) \qquad (2.6.7)$$

and considering the equations (2.6.23) and (2.6.6)

$$f'.F = (1 - f.F) = (1-f)^2 \frac{\sigma C_L}{4\sin\phi} \left(1 - \frac{C_D}{C_L} \frac{1}{\tan\phi}\right) \qquad (2.6.8)$$

Omitting the drag terms in equations (2.6.7) and (2.6.8) the following expressions yield

$$fF = (1 - fF) = \frac{\sigma C_L \cos\phi \, (1-f)^2}{4\sin^2\phi} \qquad (2.6.9)$$

$$f'F = (1 - fF) = \frac{\sigma C_L \phi \, (1-f)^2}{4\sin\phi} \qquad (2.6.10)$$

From the equation (2.6.9) and (2.6.10), the final expression for elemental thrust and torque become

$$dQ = 4fF \, (1 - fF) \left(1 + \frac{C_D}{C_L} \tan\phi\right) \rho V_\infty^3 \, \pi \, r \, d\,r \qquad (2.6.11)$$

and

$$dT = 4f'F \, (1 + fF) \left(1 - \frac{C_D}{C_L} \frac{1}{\tan\phi}\right) \rho V_\infty^2 \, 2\pi \, r^2 \, d\,r \qquad (2.6.12)$$

46

2.7 EQUATIONS FOR TOTAL THRUST, TORQUE AND POWER COEFFICIENTS

Elemental torque, thrust and power coefficients are defined as

$$d\,C_T = \frac{d\,T}{\frac{1}{2}\rho\,A\,V_\infty^2\,R} \tag{2.7.1}$$

$$d\,C_Q = \frac{d\,Q}{\frac{1}{2}\rho\,A\,V_\infty^2} \tag{2.7.2}$$

and

$$d\,C_P = \frac{d\,P}{\frac{1}{2}\rho\,A\,V_\infty^3} = \frac{d\,T\,\omega}{\frac{1}{2}\rho\,A\,V_\infty^3} \tag{2.7.3}$$

$$d\,C_P = \frac{d\,T.\omega\,R}{\frac{1}{2}\rho\,A\,V_\infty^2.\,R\,V_\infty} = d\,C_T\,\lambda \tag{2.7.4}$$

Considering the equations (2.7.1) and (2.6.12(, elemental torque coefficient can be written as

$$d\,C_T = \frac{8}{R^3}\,f'F\,(1-f.F)\left(1-\frac{C_D}{C_L}\frac{1}{\tan\phi}\right)r^2\,d\,r \tag{2.7.5}$$

Again from equation (2.7.2) and (2.7.11), elemental thrust coefficient is given by

$$d\,C_Q = \frac{8}{R^2}\,f'F\,(1-f.F)\left(1+\frac{C_D}{C_L}\tan\phi\right)r\,d\,r \tag{2.7.6}$$

Elemental power coefficient can be obtained from equation (2.7.3) as

47

$$d C_P = \frac{8 \omega}{R^2 V_\infty} f' F (1 - fF) \left(1 - \frac{C_D}{C_L} \frac{1}{\tan\phi}\right) r^2 \, d r \qquad (2.7.7)$$

Finally, total torque, thrust and power coefficients can be obtained by the following equations:

$$C_T = \frac{8}{R^3} \int_0^R f' F (1 - fF) \left(1 - \frac{C_D}{C_L} \frac{1}{\tan\phi}\right) r^2 \, d r \qquad (2.7.8)$$

$$C_Q = \frac{8}{R^2} \int_0^R fF (1 - fF) \left(1 - \frac{C_D}{C_L} \frac{1}{\tan\phi}\right) r \, d r \qquad (2.7.9)$$

$$C_P = \frac{8}{R^2} \frac{\omega}{V_\infty} \int_0^R f' F (1 - fF) \left(1 - \frac{C_D}{C_L} \frac{1}{\tan\phi}\right) r^2 \, d r \qquad [2.7.9]$$
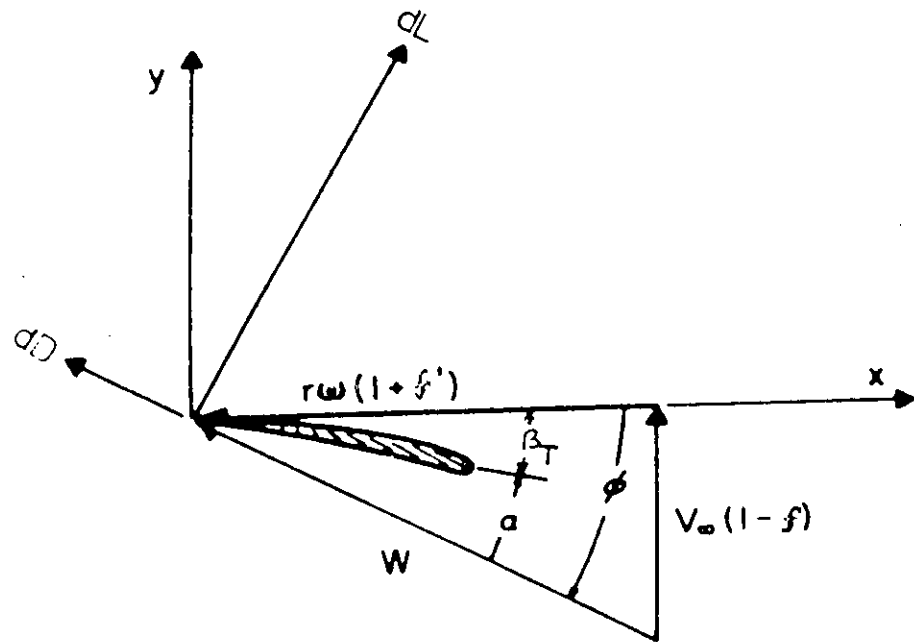
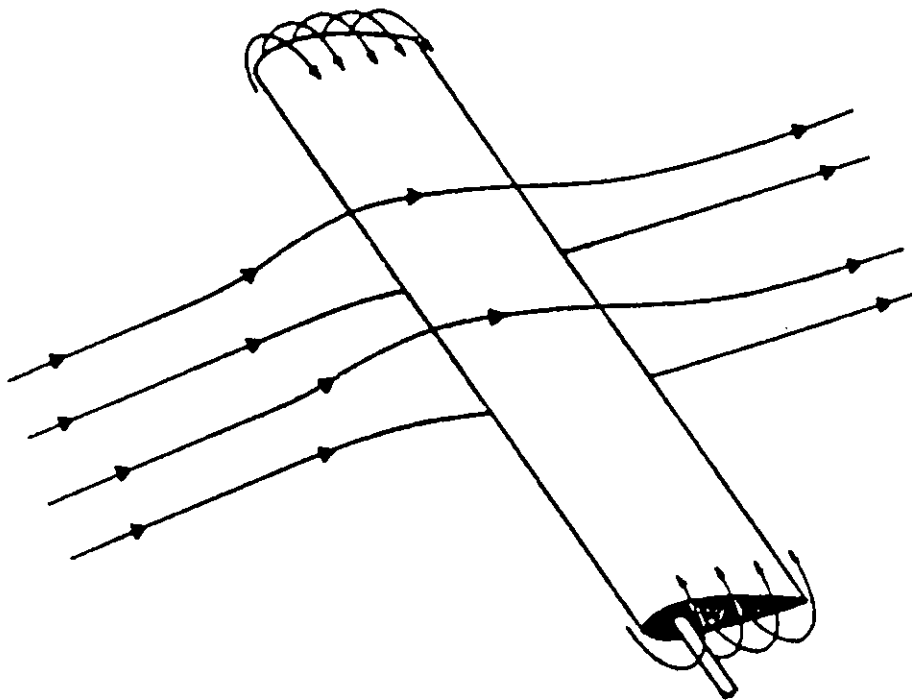Figure 2.4.1 : Velocity Diagram of a Blade Element.

Figure 2.6.a : Tip and Hub Losses Flow Diagram

CHAPTER-3

DESCRIPTION OF EXPERIMENTAL PROCEDURE ON WIND TURBINE

The experiments on the wind turbine are to be carried out in the project laboratory with the wind tunnel. The high velocity air flows through the wind tunnel when propeller type air fan is operated with the motor. The air velocity can vary by a ventilator which place in front of the propeller. The air velocity leaving from the wind tunnel are turbulent flow and this high velocity air is used as the natural air flow to rotate the wind turbine. There have many process to measure this air velocity leaving from the wind tunnel. In this experiment the air velocity is determined directly by anemometer which is placed in front of the plane of the wind turbine blades. The velocity of air at different points in front of the plane of the wind turbine blades are determined and the average velocity, V_∞ is determined from these measured velocity calculated from anemometer reading. Different average velocities $V_{\infty 1}$, $V_{\infty 2}$ & $V_{\infty 3}$ are determined by these process. These velocities are used to determined the different characteristics of the wind turbine. To determine the different characteristics of the wind turbine, a lever with brake is used for torque measurement and a tachometer is used to measure the revolution of the wind turbine. The wind turbine is tested at different air velocity and at different speed of the turbine to determine coefficient of power (C_p), torque coefficient (C_T) and P-N, C_p-λ, C_T-λ characteristics. From this test data, the wind turbine can be replaced by an electric motor by comparing the characteristics of wind turbine to the characteristics of a motor. With these simulated system either a wind pump or an electricity generator can be coupled.

To determine the characteristics of an electric motor (compound) a brake mechanism is used for measuring torque, and power at different speed and input voltage. From this tested data, different P-N curves at different input voltage are drawn. These

characteristics curves are drawn in such a way that their power and speed limits are closed to the power and speed limits of the wind turbine. From such condition, the wind turbine can be replaced by whose characteristics are known easily.

In this experiment, the following assumptions are underlying for the horizontal axis wind turbine:

i. The fluid is inviscid and incompressible.

ii. The flow velocity, V is constant at any point far ahead of the rotor blade.

iii. All blades are same size, shape and same angle of attack.

iv. Flow is entirely axial.

v. Thrust loading is uniform over the disc.

vi. Static pressure far ahead and far behind the rotor are equal to the undisturbed ambient static pressure.

vii. The rotational speed of the rotor are uniform.

3.1 DETERMINATION OF AIR DENSITY

The power of the wind turbine depends on the air density. The air density can be determined directly by the barometers reading. The air density depends on the many factors such as air temperature, atmospheric pressure , humidity etc.

The air density is determined in Appendix- L.

3.2 DETERMINATION OF C_P, C_T AND λ FOR THE THREE BLADED-WIND TURBINE AND SIX BLADED WIND TURBINE

Experimentally, the performance characteristics of the wind turbine can be measured at different way. The most suitable method is the brake mechanism system (Fig. 3.2.1). The brake mechanism are used to determine the torque on the turbine shaft. Two brake shoe made of wood, are fastened on the turbine shaft and two nut-bolt are used to apply different frictional resistance on the shaft. A lever arm is used to hang the dead load at the different point on the lever arm to balance the frictional resistance. In balance condition, the product of the dead load and lever arm length the torque applied on the shaft.

The following data are for the three bladed and six bladed wind turbine:

Radius of the wind turbine blades, R = 30 cm

Turbine swept area, $A = \pi R^2 = \pi \left(\dfrac{30}{100}\right)^2$

$A = 0.283 \text{ m}^3$
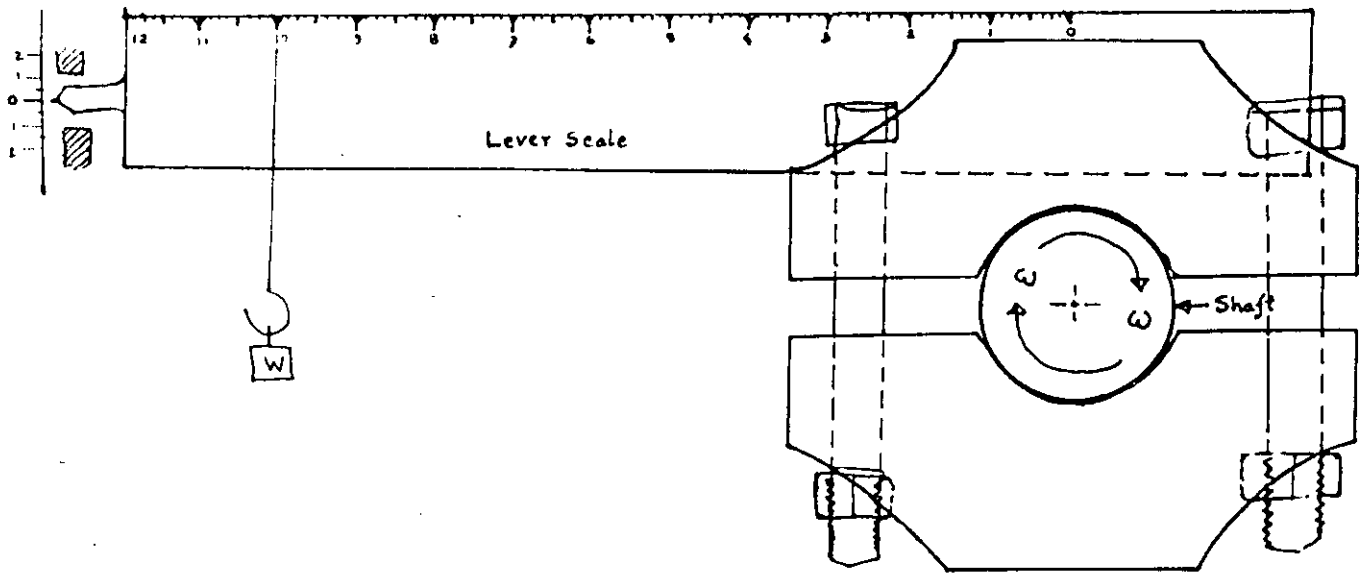
Figure 3.2.1: The brake mechanism to measure torque of the turbine shaft.

53

Applied torque on the turbine shaft, T = Dead load x Arm length

$$T = W \times L$$

Angular velocity of the turbine shaft, $\omega = \dfrac{2\pi N}{60}$

where, N = revolution per minute of the turbine shaft.

Wind velocity = V_∞

Shaft power of the turbine $P = T \times \omega$

$$P = (W \times L) \times 2\pi N/60 \qquad (3.2.1)$$

The power coefficient is defined as

$$C_p = \frac{P}{\dfrac{1}{2}\rho A V_\infty^3}$$

$$\therefore C_p = \frac{(W \times L) \times \dfrac{2\pi N}{60}}{\dfrac{1}{2}\rho A V_\infty^3} \qquad (3.2.2)$$

The torque coefficient is defined as

$$C_T = \frac{T}{\dfrac{1}{2}\rho A V_\infty^2 R}$$

$$C_T = \frac{W \times L}{\dfrac{1}{2}\rho A V_\infty^2 R} \qquad (3.2.3)$$

and Tip speed ratio, $\qquad \lambda = \dfrac{\omega R}{V_\infty}$

$$\lambda = \frac{\frac{2\pi N}{60} \times R}{V_\infty} \qquad (3.2.4)$$

By knowing the value of W, L, N, ρ, A & V_∞, the value of C_p, C_T, & λ for the three bladed and six bladed wind turbine are calculated. The data of the above parameters are available in Appendix A, B,C, D, E & F. From the value of C_p and C_T at different tip speed ratio λ, the characteristics curves C_p - λ, C_T - λ are drawn

3.3   ANALYSIS OF WIND TURBINE CHARACTERISTICS

A wind rotor can extract power from the wind because it slows down the wind- not too much, not too little. At standstill the rotor obviously produces no power and at very high rotational speeds the air is more or less blocked by the rotors and again no power is produced. In between, these extremes, there is an optimal rotational speed where the power extraction is at a maximum. These is illustrated in Figure 3.3.1 and Figure 3.3.2.

It is often also interesting to know the torque- speed curve of a wind rotor, when applying torque on the rotor by a brake. The power P(watt), the torque, T (N-m) and the rotational speed ω(rad/s) and related by a simple law:

$$P = T\omega \qquad (3.3.1)$$

It may be conducted that, because $T = \dfrac{P}{\omega}$, the torque is equal to the tangent of a line through the origin and some point of the P and ω curve. This is why the maximum of the torque curve is reached at lower speeds than the maximum of the power curve. If

the wind speed increases, power and torque increases, so for each wind speed a separate curve are to be drawn, both power and for torque.

The curves in Figure 3.3.1, Figure. 3.3.2, Figure. 3.3.3 and Figure. 3.3.4 are rather inconvenient to handle as they vary with the wind speed V_∞, the radius R of the turbine and even the dimensionless with the following expressions:

$$\text{Power coefficient,} \quad C_p = \frac{P}{\frac{1}{2}\rho A V_\infty^3}$$

$$\text{Torque coefficient,} \quad C_T = \frac{T}{\frac{1}{2}\rho A V_\infty^2 R}$$

$$\text{Tip speed ratio,} \quad \lambda = \frac{\omega R}{V_\infty}$$

The immediate advantage is that the behaviour of the turbine with different dimensions and at different wind speeds can be reduced to two curves: C_P - λ and C_T - λ. One significant difference between six bladed turbine and three bladed turbine is Figure 3.3.5 and Figure 3.3.6 is that six bladed turbine operate at low Tip speed ratios are three-bladed turbine operate at high tip speed ratios. The advantages of increasing the number of blades are improved performance and lower torque variation due to wind shear. The maximum power coefficient is also affected by the number of blades, because of the tip losses that occur at the tips of the blades. These losses depend on the number of blades and tip speed ratios. For the lower design tip speed ratios, generally a high number of blades is chosen. This is done because the influence of number of blades on power coefficient is larger at lower tip speed ratios. For a high design tip speed ratio with a high number of blades will lead to very small and thin blades which results in manufacturing problems and a negative influence on the lift and drag properties of blades. Increase of number of blades shows that the

56

region of higher power coefficient move to the region of smaller values of tip speed ratios and increase of number of blades increases the solidity of the turbine. More the solidity of the turbine, the starting speed of the turbine will be less (Figure 3.3.7.).

Figure 3.3.1: The power of wind turbine as a function of rotational speed for different wind speeds for three bladed wind turbine.

Figure 3.3.2: The power of wind turbine as a function of rotational speed for different wind speeds for six bladed wind turbine.
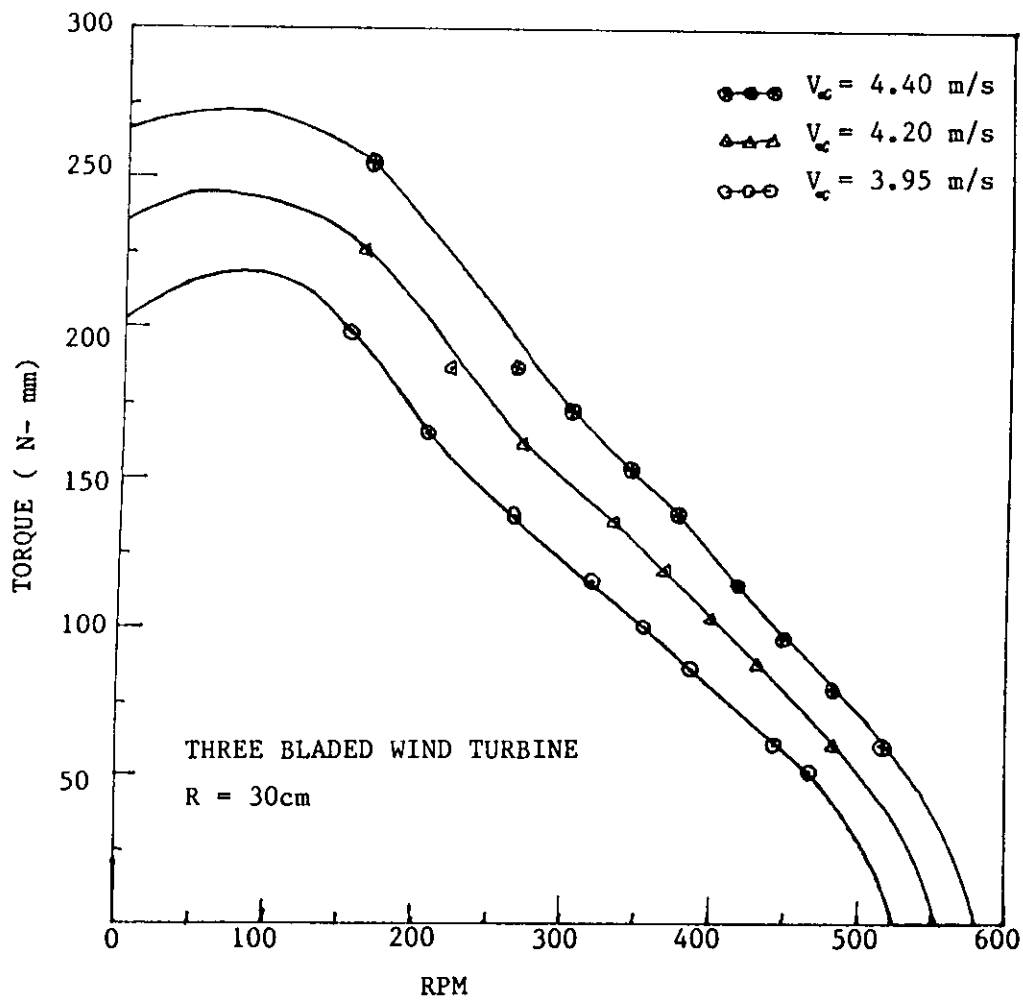
Figure 3.3.3: The torque of wind turbine as a function of rotational speed for different wind speeds for three bladed wind turbine.

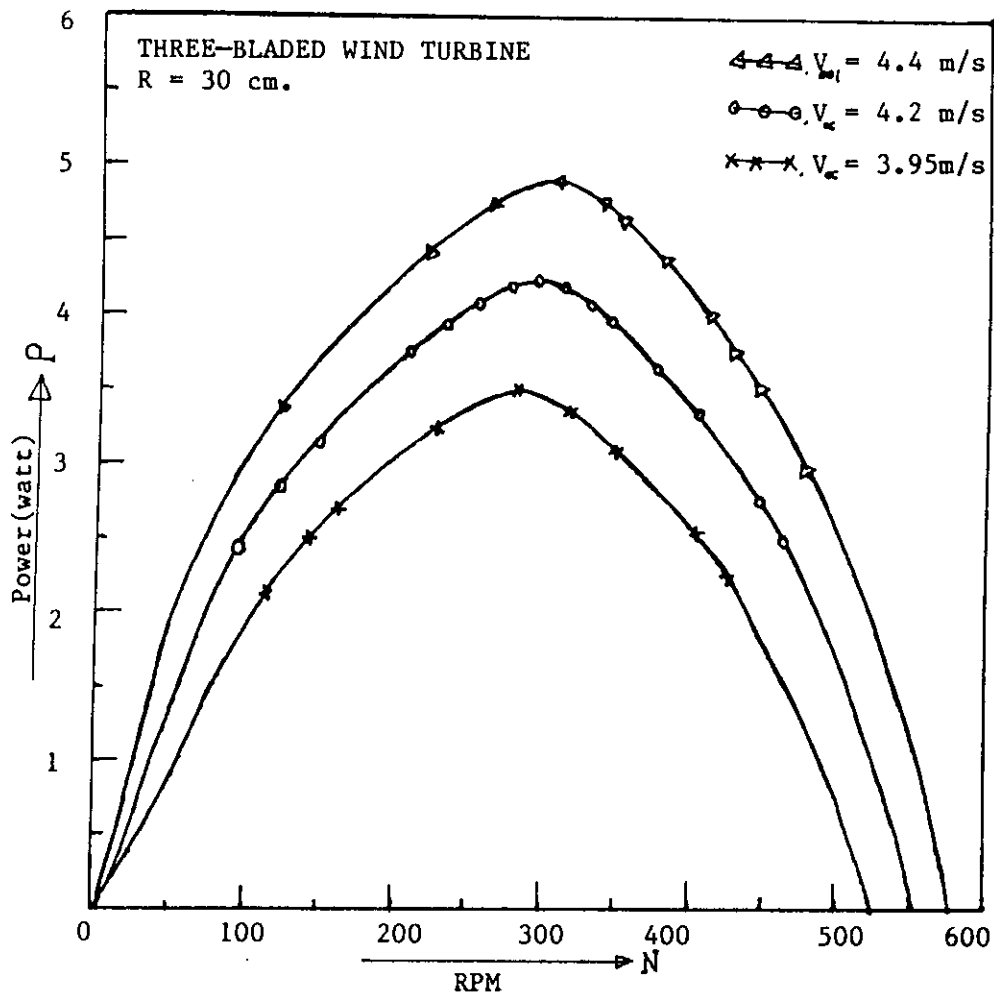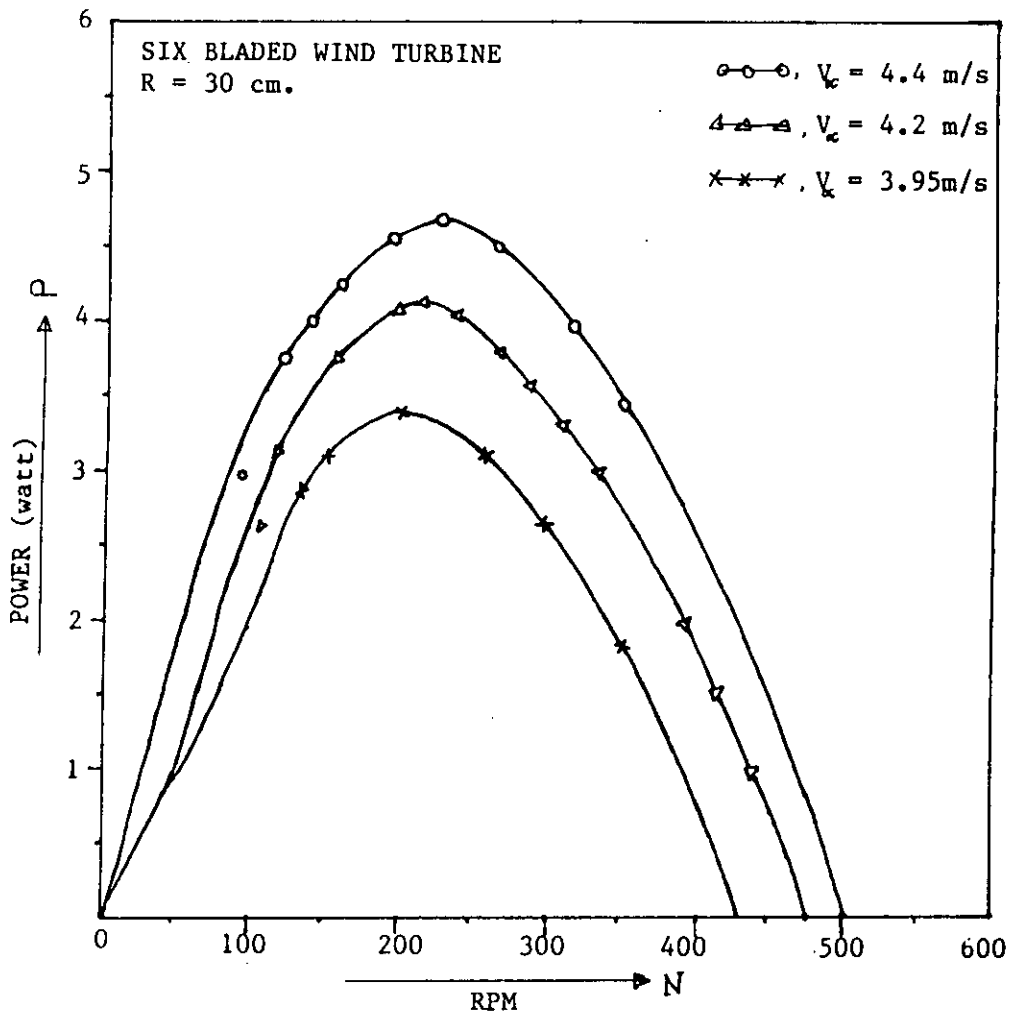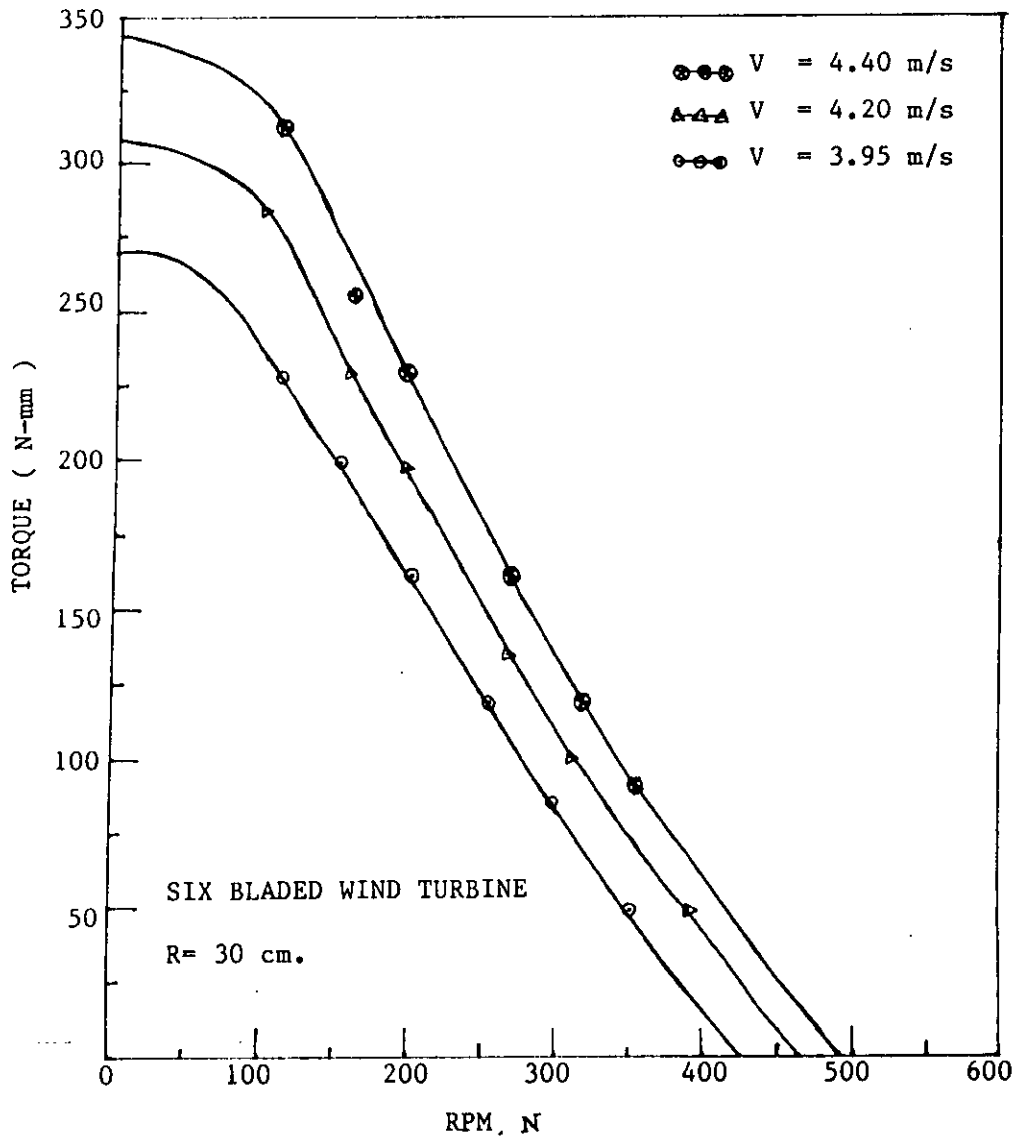Figure 3.3.4: The torque of wind turbine as a function of rotational speed for different wind speeds for six bladed wind turbine.
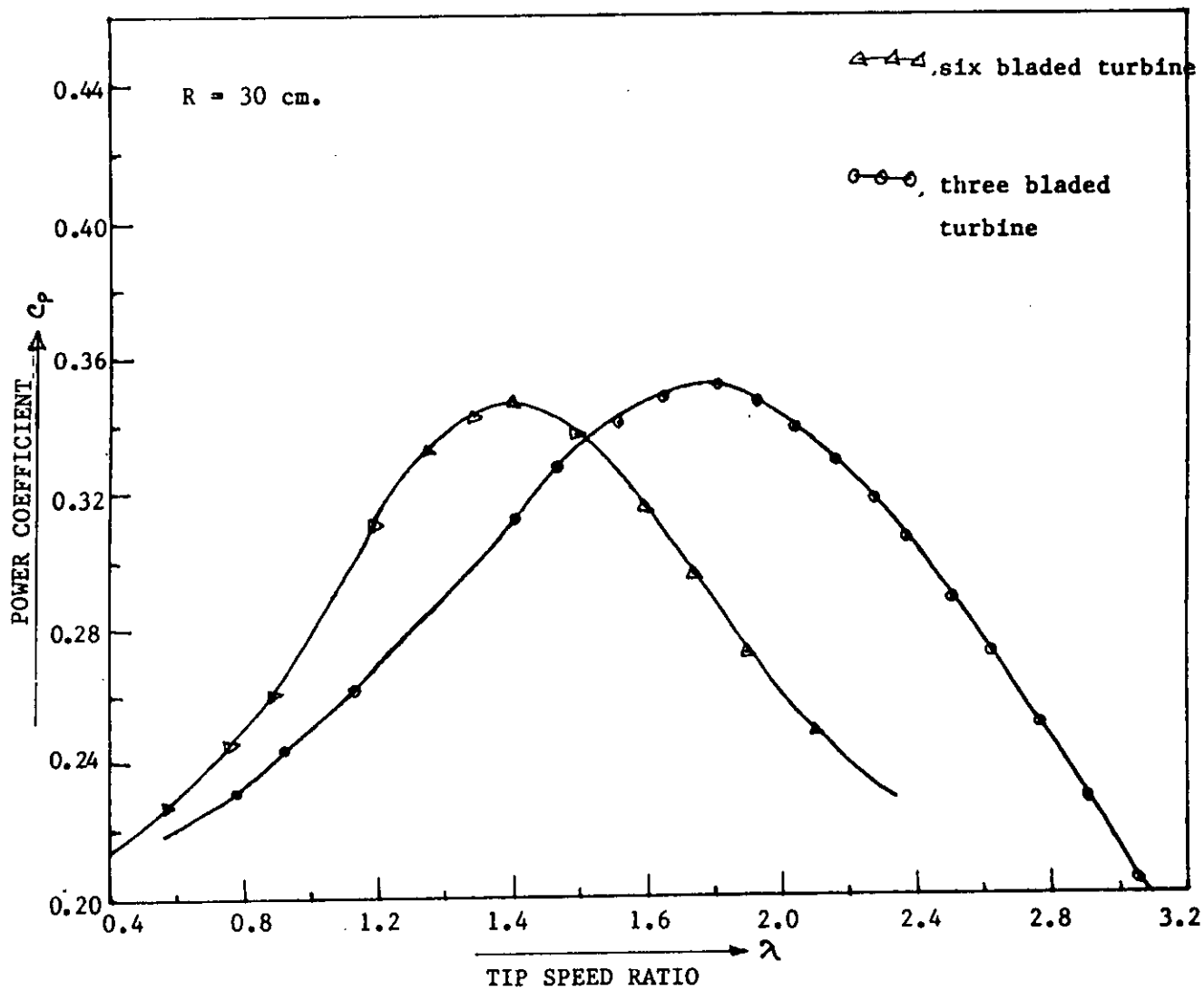
Figure 3.3.5: Variation of power coefficient with tip speed ratio.
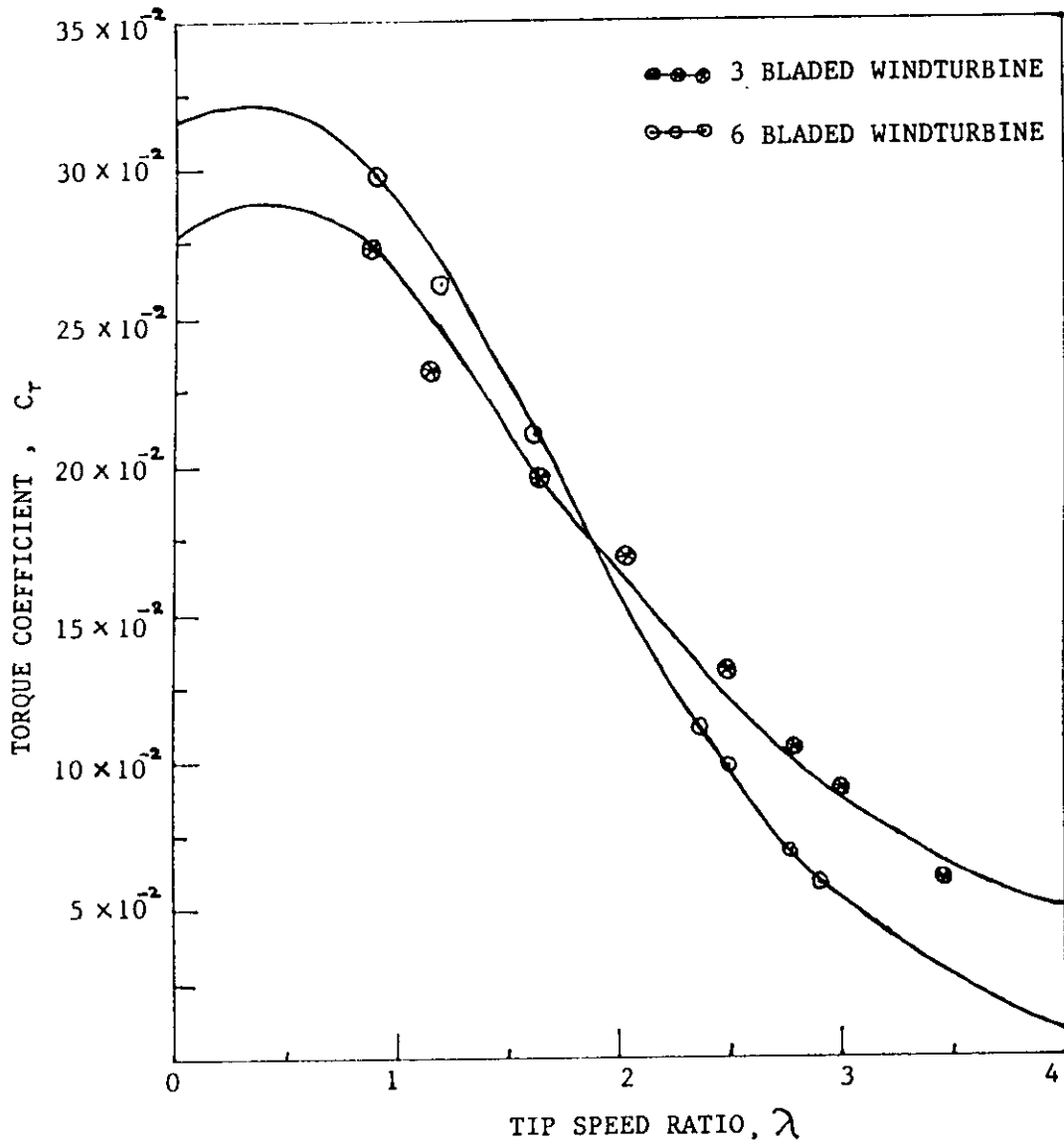
Figure 3.3.6: Variation of torque coefficient with tip speed ratio.

63
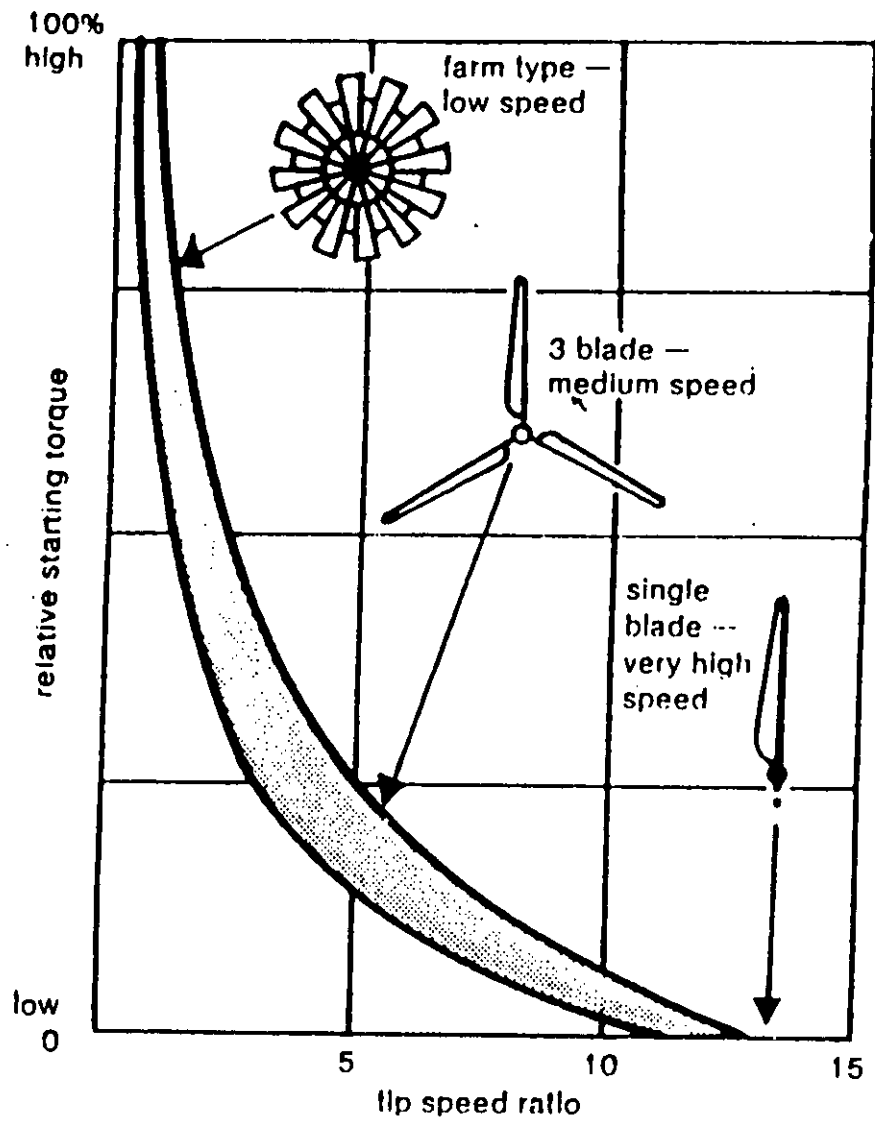
Figure 3.3.7(a): Relative starting torque(Adapted from lysen,E.H[29].)
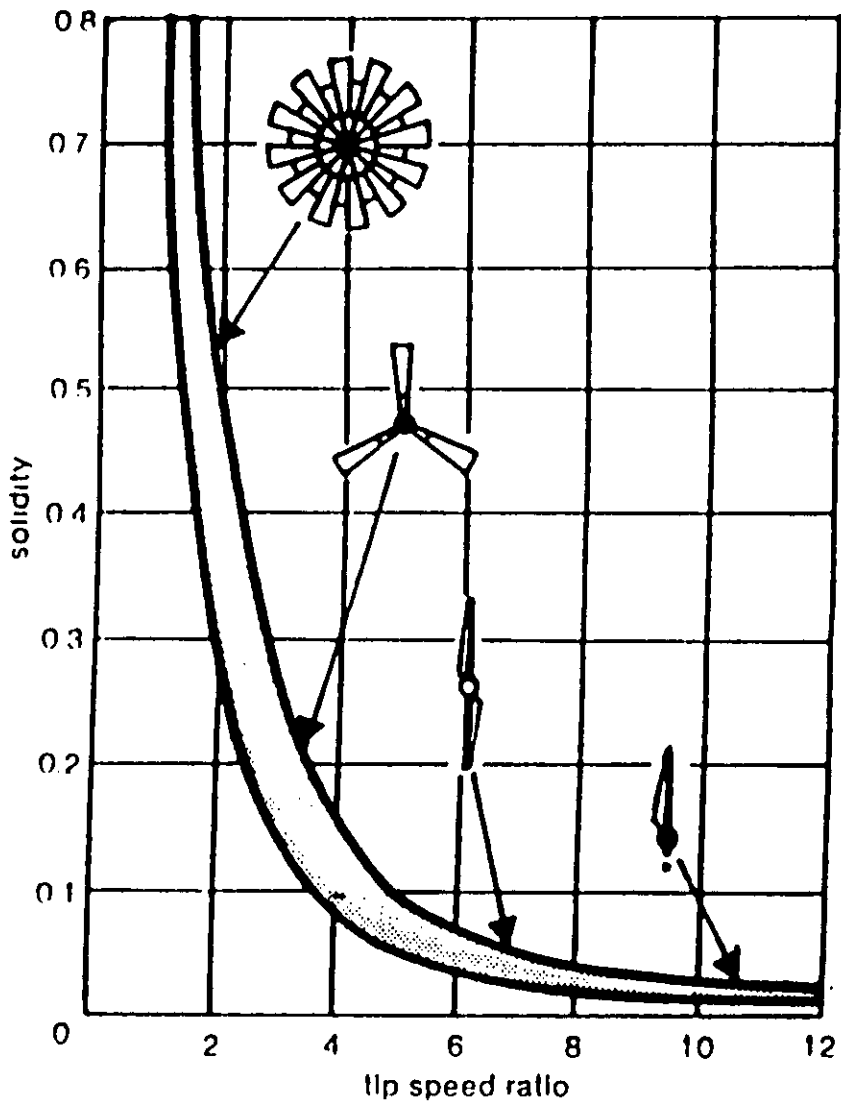
Figure 3.3.7(b): Solidity of several wind machines.(Adapted from lysen,E.H[29])

CHAPTER-4

ELECTRIC MOTOR AND ITS SIMULATION WITH WIND TURBINE

4.1   ELECTRIC D. C. MOTOR

An electric motor is a machine which converts electric energy into mechanical energy. Its action is based on the principle that when a current-carrying conductor is placed in a magnetic field, it experiences a mechanical force whose direction is given by Fleming's Left-hand Rule and whose magnitude is given by F=BIL Newton. Constructionally, there is no basic difference between a D. C. generator and a D. C. motor. In fact, the same d.c. machine can be interchangeably as a generator or as a motor. D. C. motors are also like generators, shunt-wound or series-wound or compound wound.

In Fig. 4.1.1(a) is shown a part of a multipolar D. C. motor. When its field magnets are excited and its armature conductors are supplied with current from the supply mains, they experience a force tending to rotate the armature. Armature conductors under N-pole are assumed to carry current downwards (crosses) and those under S-poles to carry current upwards (dots).

By applying Fleming's Left-hand Rule, the direction of the force on each conductor can be found. It is shown by small arrows placed above each conductor. It will be seen that each conductor experiences a force F which tends to rotate the armature in anticlockwise direction. These forces collectively produce a driving torque which

sets the armature rotating. It should be noted that the function of a commutator in the motor is the same as in a generator. By reversing current in each conductor as it passes from one pole to another, it helps to develop a continuous and unidirectional torque. A D. C. Machine can be used, at least theoretically, interchangeably as a generator or as a motor. When operating as a generator, it is driven by a mechanical machine and it develops voltage which inturn produces a current flow in an electric circuit. When operating as a motor, it is supplied by electric current and it develops torque which inturn produces mechanical rotation. As soon as the armature starts rotating, dynamically induced e.m.f is produced in the armature conductors. The direction of this induced e.m.f as found by Fleming's Right-hand Rule, outwards i.e. in direct opposition to the applied voltage Figure 4.1.1(b). That is why it is known as back e.m.f, E_b or counter e.m.f. Its value is the same as for the motionally induced e.m.f in the generator i.e. $E_b = (\frac{\phi Z N}{60}) \times (P / A)$ volts. The applied voltage V_c has to force current through the armature conductors against this back e.m.f, E_b. The electric work done in overcoming this opposition is converted into mechanical energy developed in the armature. Therefore, it is obvious that for the production of this opposing e.m.f energy conversion would not have been possible. It is seen that in an actual motor with slotted armature, the torque is not due to mechanical force on the conductors themselves, but due to tangential pull on the armature teeth as shown in Figure 4.1.2. In Figure 4.1.2(c), the main flux is concentrated in the form of tufts at the armature teeth while the armature flux is shown by the dotted lines embracing the armature slots. The effects of armature flux on the main flux as shown in Figure 4.1.2(d), is two-fold:

i.   It increases the flux on the left-hand side of the teeth and decreases it on the right-hand side, thus making the distribution of the flux density across the tooth section unequal.

ii.   It inclines the direction of lines of force in the air-gap so that they are not radial but are disposed in a manner in Figure 4.1.2(d). The pull exerted by the poles on the teeth can now be resolved into two components. One is the tangential component F_1 and the other vertical component F_2. The vertical component F_2, when considered for all the teeth round the armature adds upto zero. But the component F_1 is not cancelled and it is this tangential component which acting on all the teeth, gives rise to the armature torque.

When the motor armature rotates, the conductors also rotate and hence cut the flux. In accordance with the laws of electromagnetic induction, e.m.f is induced in them whose direction, as found by Fleming's Right-hand Rule, is in opposition to the applied voltage (Figure 4.1.3). Because of its opposing direction it is referred to as counter e.m.f or back e.m.f E_b.

The equivalent circuit of a motor is shown in Figure 4.1.3(f). The rotating armature generating the back e.m.f E_b is like a battery of e.m.f E_b put across a supply mains of V_e volts. Obviously, V_e has to drive I_a against opposition of E_b. The power required to overcome this opposition is $E_b I_a$. In the case of a cell, this over an interval of time is converted into chemnical energy, but in the present case, it is converted into mechanical energy. It will be seen that $I_a = \dfrac{\text{net voltage}}{\text{resis} \tan \text{ce}} = \dfrac{V_e - E_b}{R_a}$ where R_a is the resistance of the armature circuit and $E_b = (\dfrac{\phi Z N}{60}) \times (P / A) \text{volt}$ where N is in rpm.

Back e.m.f depends, among other factors, upon the armature speed. If speed is high, E_b is large hence armature current I_a is small. If the speed is less, then E_b is less, hence more current flows which develops more torque. So we find that E_b acts like a

governor i.e. it makes a motor self-regulating so that it draws as much current as in just necessary.

The voltage V_c applied across the motor armature has to

(i) overcome the back e.m.f E_b and

(ii) supply the armature ohmic drop I_aR_a

$$\therefore \quad V_c = E_b + I_aR_a$$

This is known as voltage equation of a motor. Hence, out of the armature input, some is waste in I^2R loss and the rest is converted into mechanical power within the armature. It may also be noted that motor efficiency is given by the ratio of power developed by the armature to its input i.e. $\dfrac{E_bI_a}{V_eI_a} = \dfrac{E_b}{V_c}$. Obviously, higher the value of

Eb as compared to V_c, higher the motor efficiency. The gross mechanical power developed by a motor is

$$P_m = V_cI_a - I_a^2R_a$$

Differentiating both sides with respect to I_a and equating the result to zero, we get

$$\frac{dP_m}{dI_a} = V_c - 2I_aR_a = 0$$

$$\therefore \quad I_aR_a = \frac{V_c}{2}$$

$$\text{As} \quad V_e = E_b + I_aR_a = E_b + \frac{V_c}{2}$$

$$\therefore \quad E_b = \frac{V_c}{2}$$

Thus gross mechanical power developed by a motor is maximum when back e.m.f is equal to half the applied voltage. This condition is however, not realized in practice, because in that case current would be much beyond the normal current of the motor. Moreover, half the input would be wasted in thr form of heat and taking other losses
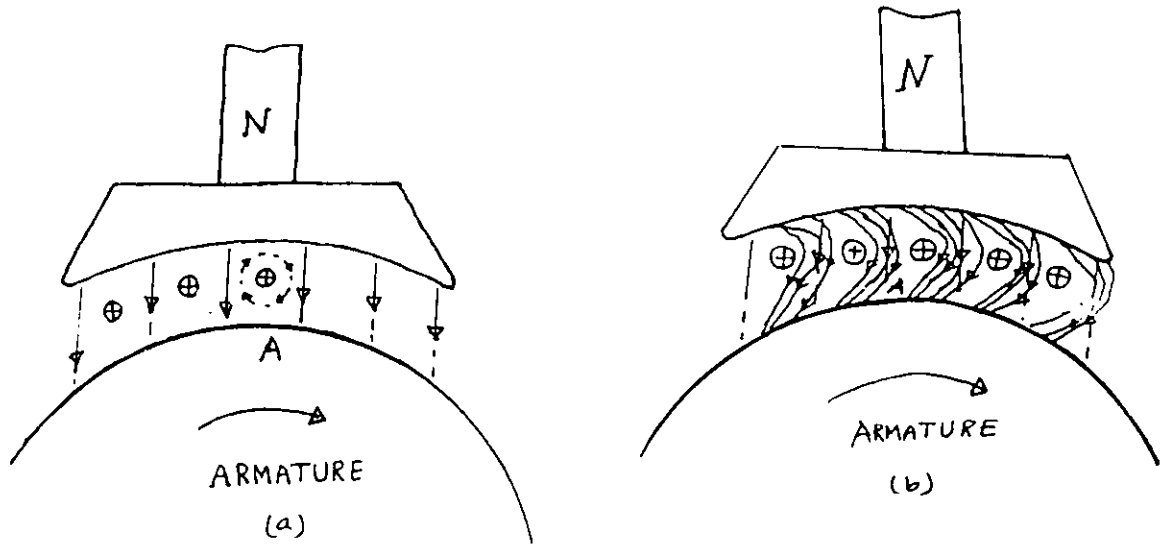
Figure 4.1.1
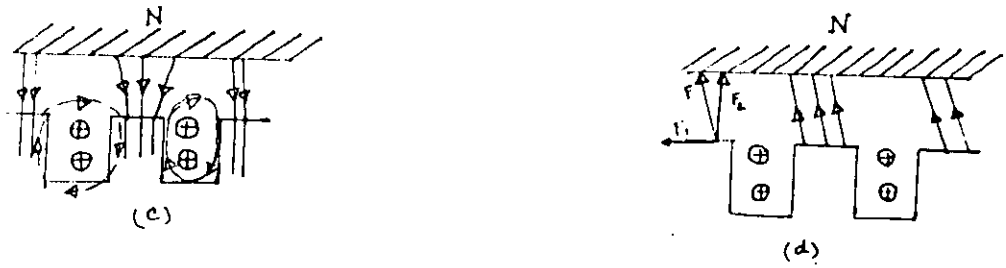
Figure 4.1.2
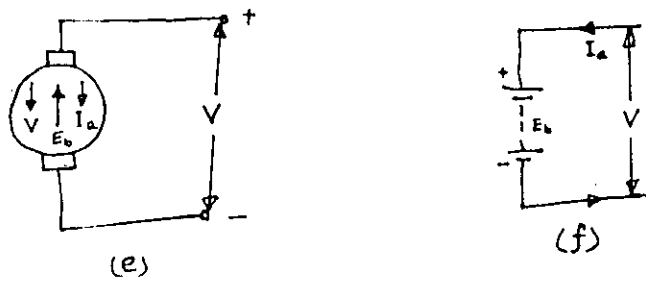
Figure 4.1.3

(Mechanical and Magnetic) into consideration, the motor efficiency will be well below 50 percent.

4.2 EXPERIMENTAL PROCEDURE ON D.C. MOTOR TO DETERMINE ITS CHARACTERISTICS

In this experiment, a D. C. compound motor is tested at different input voltage and different applied torque exerted by a brake mechanism on the motor shaft. At particular input voltage, the speed and armature current of the motor vary with various applied torque on the motor shaft. If the applied torque on the motor shaft increases, the speed decreases and vise-versa. Similarly, the armature current increases with increase of applied torque. So the D. C. motor is tested at different applied torques to obtain the different speed of the motor and from this tested data, the characteristics curves P-N are drawn at particular input voltage. Similarly by changing the input voltage, a set of P-N curves are obtained.

The power and torque of the motor depends on the armature current Ia. If the armature current Ia increases, the power and torque increases. So at particular input voltage, if the load on the motor increases, the armature current increases because of the decreasing the motor speed, that is decreasing the back e.m.f. The relation between power and speed of the motor are shown in Figure 4.2.1. The figure shows that as the increase of input voltage the P-N curve shift to the higher speed and the power ranges and speed ranges are increased. Again the increase of input voltage of the motor, the speed of the motor become more stable with different applied shaft torque and the variation of speed with power become more linearity.

71

In this experiment, the motor is tested in such power and speed ranges so that the characteristics curves of the motor can be compared to the characteristics curves of the wind turbine. From this characteristics comparison, the simulation system between wind turbine and D. C. motor are found:

4.3   SIMULATION SYSTEM OF WIND TURBINE AND D. C. MOTOR

From different characteristics curves, it is observed that the power of the wind turbine at any particular speed is depend on the wind velocity. Similarly the speed of the wind turbine at any particular power is depend on the wind velocity and the power of the turbine increases with the increase of the wind velocity. Again at any particular wind velocity, the power of the wind turbine varies with the change of turbine speed and at one particular turbine speed, the power of the wind turbine is maximum. Similarly, at another wind velocity, the turbine speed at maximum turbine power changes to another value. So, the increase of wind velocity, the region of higher turbine power move to the region of higher values of turbine speeds. Again, the relation between turbine power and speed depend on the number of blades of the wind turbine. More the number blades of the wind turbine, the wind turbine operates at low tip speed ratio. So, the six bladed wind turbine operates at low tip speed ratio and the three bladed wind turbine operate at high tip speed ratio. The advantage of increasing the number of blades are improved performance and lower torque variation due to wind shear. The maximum power coefficient is also affected by the number of blades, because of the tip losses that occur of the tips of the blades. These losses depend on the number of blades and tip speed ratios. For the lower design tip speed ratios, generally a high number of blades is chosen. This is done because the influence of number of blades on power

72

coefficient is larger at lower tip speed ratios. TIhe increase of number of blades shows that the region of higher power coefficient move to the region of smaller values of tip speed ratio.

On the otherhand, at any particular voltage, the shaft power of the motor varies with the change of motor speed. If the speed of the motor increases, the power of the motor decreases. Again the increase of the input voltage of the motor, the higher power region moves to the higher speed region in the power-speed curve. So different power-speed curves are obtained by varying the input voltage of the motor and these curves are used to obtain the actual motor specification by simulation system for use instead of a wind turbine.

In the simulation system, the different characteristics of the wind turbine are compared with the characteristics of the electric motor which are shown in figure 4.3.1 and figure 4.3.2. In figure 4.3.1, the P-N characteristics curves of the three-bladed wind turbine are compared to the P-N characteristics curves of the electric motor and in figure 4.3.2, the P-N characteristics curves of the six-bladed wind turbine are compared to the P-N characteristics curves of the electric motor. From these comparison, it can be easily estimate that whether the motor drive are suited with the wind turbine drive at different wind velocities.

From the P-N characteristics curve in Figure 3.3.1 for three bladed wind turbine, it is shown that at the wind velocity $V_\infty = 3.95$ m/s, the maximum power, $P_{max} = 3.48$ watts is obtained from the wind turbine at the turbine speed N = 280 rpm when the exerted torque on the shaft is T = 118.71 N-mm, the applied torque T = 118.71 N-mm on the shaft is constant, then the power

73

and the speed of the wind turbine fall as the wind velocity decreases. Similarly the power and the speed of the wind turbine increases at constant torque as the wind velocity increases.

From Figure 3.3.1, if the constant torque on wind turbine shaft is T = 118.71 N-mm then the power obtain from different wind velocities are as follows:

DATA TABLE - 1

No. of Observation	Wind Velocity $(V_\infty(m/s)$	T Constant torque (N-mm)	N Turbine speed (rpm)	P Power (watt)	ΔP (Change of power from operating power) (Watt)
1	3.95	118.71	280	3.48	- 0.573
2	4.20	118.71	326	4.053	0
3	4.40	118.71	365	4.50	+ 0.447

If we consider the speed N = 326 rpm as the operating speed of the wind turbines then for the constant applied torque T = 118.71 N-mm the speed of the turbine decreases as the wind velocity decreases and the speed of the turbine increases as the wind velocity increases. So, from Data Table-1, it is shown that when the wind velocity decreases from 4.2 m/s to 3.95 m/s, the speed of the turbine decreases from 3.26 rpm to 280 rpm due to power fall from 4.053 watt to 3.48 watt and similarly when the wind velocity increase from 4.20 m/s to 4.40 m/s the speed of the turbine increase from 326 rpm to 365 rpm due to power rise from 4.053 watt to 4.50 watt. This variation of power from the operating power P = 4.053 watt, can be removed by the power simulation system where a D.C motor are coupled and run at the same operating conditions of the wind turbine. If the power of the wind turbine fall due to the decrease of wind velocity, then the motor is able to supply this shortfallen of power to the wind turbine by suitable belt drive. Again if the

74

power of the wind turbine rise due to the increase of wind velocity, then the extra-power of the wind turbine are supplied to the motor shaft for further utilization. In this simulation system, the addition of power from the motor shaft to the wind turbine shaft due to decrease of wind velocity can be find out experimentally by applying additional torque on the motor shaft. Similarly in this system, the reduction of power from the motor shaft when the power of the wind turbine increase due to increase of wind velocity can be find out by substracting the torque from the motor shaft.

The addition of power from the motor shaft to the wind turbine due to decrease of wind velocity are measured by the following experimental procedure where the terminal voltage of the motor is 41 volt AC:

DATA TABLE - 2

No. of Observation	Initial torque (Torque applied by First brake) (N-mm)	Additional torque (N-mm)	Total torque (N-mm)	N Speed (rpm)	P Power (watt)	ΔP Variation of power (Watt)
1	118.71	0	118.71	326	4.053	0
2	118.71	8.48	127.19	317	4.220	+ 0.167
3	118.71	16.96	135.67	308	4.40	+ 0.347
4	118.71	42.39	161.10	289	4.87	+ 0.817
5	118.71	54.54	173.25	280	5.08	+ 1.027

Again, the reduction of power from the motor shaft when the power of the wind turbine increase due to increase of wind velocity are measured by following experimental procedure where the terminal voltage of the motor is 41 volt AC:

No. of Observation	Initial torque (Torque applied by First brake) (N-mm)	Additional torque (N-mm)	Total torque (N-mm)	N Speed (rpm)	P Power (watt)	ΔP Variation of power (Watt)
1	118.71	0	118.71	326	4.053	0
2	118.71	- 8.00	110.72	336	3.89	0.163
3	118.71	- 17.48	101.23	345	3.65	0.403
4	118.71	- 24.96	93.75	354	3.46	0.593
5	118.71	- 33.92	84.79	365	3.22	0.833

Now the characteristics curves (Figure 4.3.3) drawn from the Data Table-1, Data Table-2 and Data Table-3 show the power simulation system where any fall of the power of the wind turbine from the operating point are the image of the power increase of the motor from the operating point. Similarly this characteristics curves show the power simulation system where any increase of the power of the wind turbine from the operating point are the image of the power decrease of the motor from the operating point.

From the P-N characteristics curves in Figure 3.3.2 for six bladed wind turbine, it is shown that at the wind velocity, V_{∞} = 3.95 m/s, the maximum power P_{max} = 3.425 watts are obtained from the wind turbine at the turbine speed N = 200 rpm when the exerted torque on the shaft is T = 161.10 N-mm. If the applied torque T = 161.10 N-mm on the shaft is constant, then the power and the speed of the wind turbine fall as the wind velocity decreases. Similarly the power and the speed of the wind turbine increase at constant torque as the wind velocity increase.

From Figure 3.3.2, if the constant torque on wind turbine shaft is T = 161.10 N-mm then the power obtains from different wind velocity are as follows:

DATA TABLE - 4

No. of Observation	Wind Velocity (Vₒ(m/s)	T Constant torque (N-mm)	N Turbine speed (rpm)	P Power (watt)	ΔP (Change of power from operating power) (Watt)
1	3.95	161.10	200	3.425	- 0.622
2	4.20	161.10	237	4.047	0
3	4.40	161.10	266	4.489	+ 0.442

If we cosider the speed N = 237 rpm as the operating speed of the wind turbines then for the constant applied torque T = 161.10 N-mm the speed of the turbine decreases as the wind velocity decreases and the speed of the turbine increases as the wind velocity increases. So from Data Table-4, it is shown that when the wind velocity decreases from 4.2 m/s to 3.95 m/s, the speed of the turbine decreases from 237 rpm to 200 rpm due to power fall from 4.047 watts to 3.425 watts and similarly when the wind velocity increases from 4.20 m/s to 4.40 m/s the speed of the turbine increases from 237 rpm to 266 rpm due to power rise from 4.047 watts to 4.489 watts. This variation of power from the operating power, P = 4.047 watt can be removed by the power simulation system where a D.C motor are coupled and run at the same operating conditions of the wind turbine. If the power of the wind turbine falls due to the decreases of wind velocity, Then the motor can be able to supply this shortfallen of power to the wind turbine by suitable belt drive. Again, if the power of the wind turbine rise due to the increase of wind velocity then the extra power of the wind turbine are supplied to the motor shaft for further utilization. In this simulation system, the addition of power from the motor shaft to the wind turbine shaft due to decrease of wind

velocity, can be find out experimentally by applying additional torque on the motor shaft. Similarly in this system, the reduction of power from the motor shaft when the power of the wind turbine increase due to increase of wind velocity can be find out by substracting the torque from the motor shaft.

The addition of power from the motor shaft to the wind turbine due to decrease of wind velocity are measured by the following experimental procedure where the terminal voltage of the motor is 33.5 Volt AC:

DATA TABLE - 5

No. of Observation	Initial torque (Torque applied by First brake) (N-mm)	Additional torque (N-mm)	Total torque (N-mm)	N Speed (rpm)	P Power (watt)	ΔP Variation of power (Watt)
1	161.10	0	161.10	237	4.047	0
2	161.10	22.61	183.71	225	4.38	+ 0.333
3	161.10	36.75	197.85	218	4.50	+ 0.453
4	161.10	50.88	211.98	211	4.70	+ 0.653
5	161.10	73.81	234.91	200	4.92	+ 0.873

Again, the reduction of power from the motor shaft when the power of the wind turbine increase due to increase of wind velocity are measured by following experimental procedure where the terminal voltage of the motor is 33.5 Volt AC:

DATA TABLE - 6

No. of Observation	Initial torque (Torque applied by First brake) (N-mm)	Reduction of torque (N-mm)	Total torque (N-mm)	N Speed (rpm)	P Power (watt)	ΔP Variation of power (Watt)
1	161.10	0	161.10	237	4.047	0
2	161.10	- 8.48	152.62	244	3.90	- 0.147
3	161.10	- 16.95	144.15	251	3.79	- 0.257
4	161.10	- 25.43	135.67	258	3.66	- 0.387
5	161.10	- 35.81	125.29	266	3.49	- 0.557

Now the characteristics curves (Figure-4.3.4) drawn from the Data Table-4, Data Table-5 and Data Table-6 show the power simulation system where any fall of the power of the wind turbine from the operating point are the image of the power increase of the motor from the operating point. Similarly this characteristics curve show the power simulation system where any increase of the power of the wind turbine from the operating point are the image of the power decrease of the motor from the operating point.
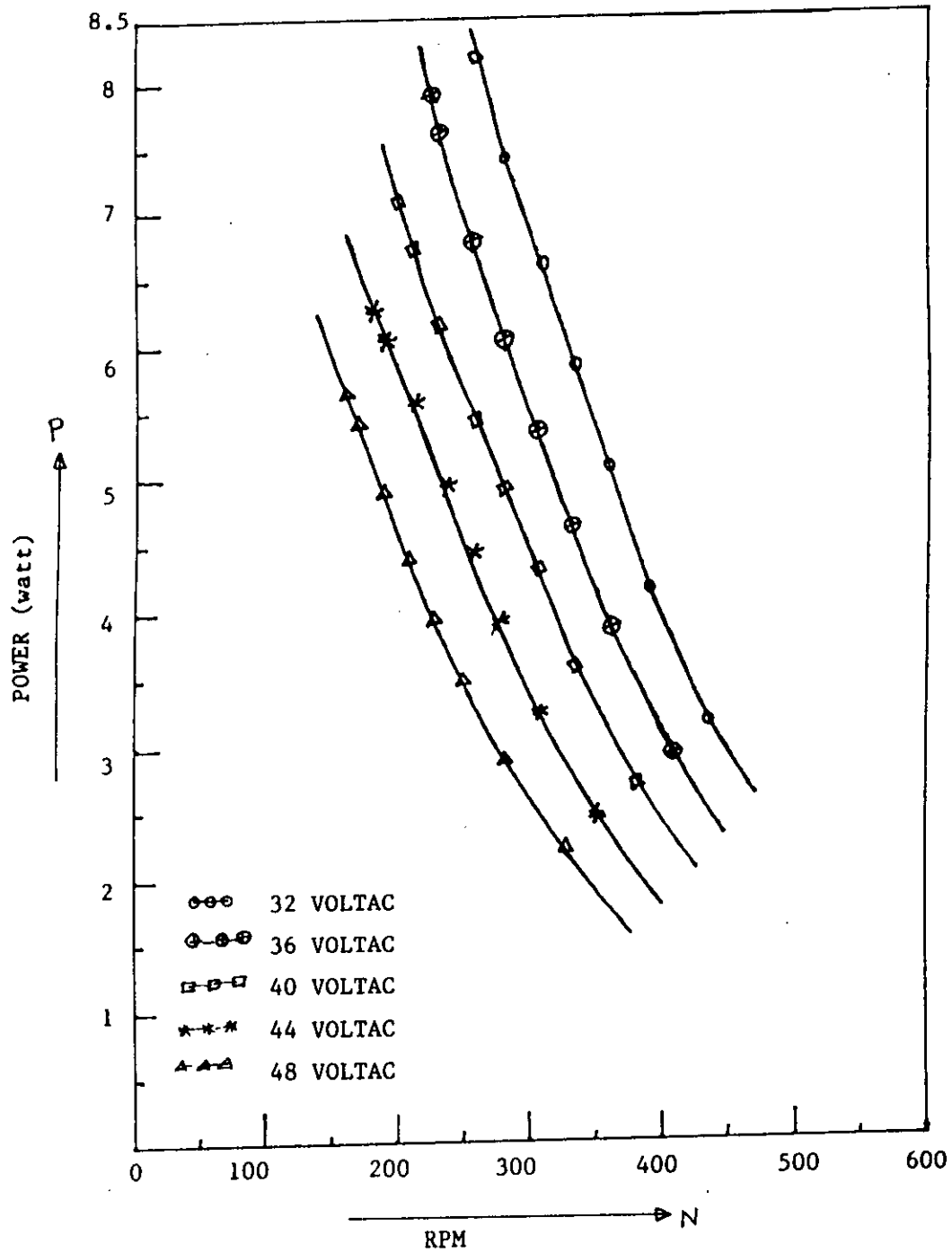
Figure 4.2.1: The power of D. C. electric motor as a function of rotational speed for different input voltage.
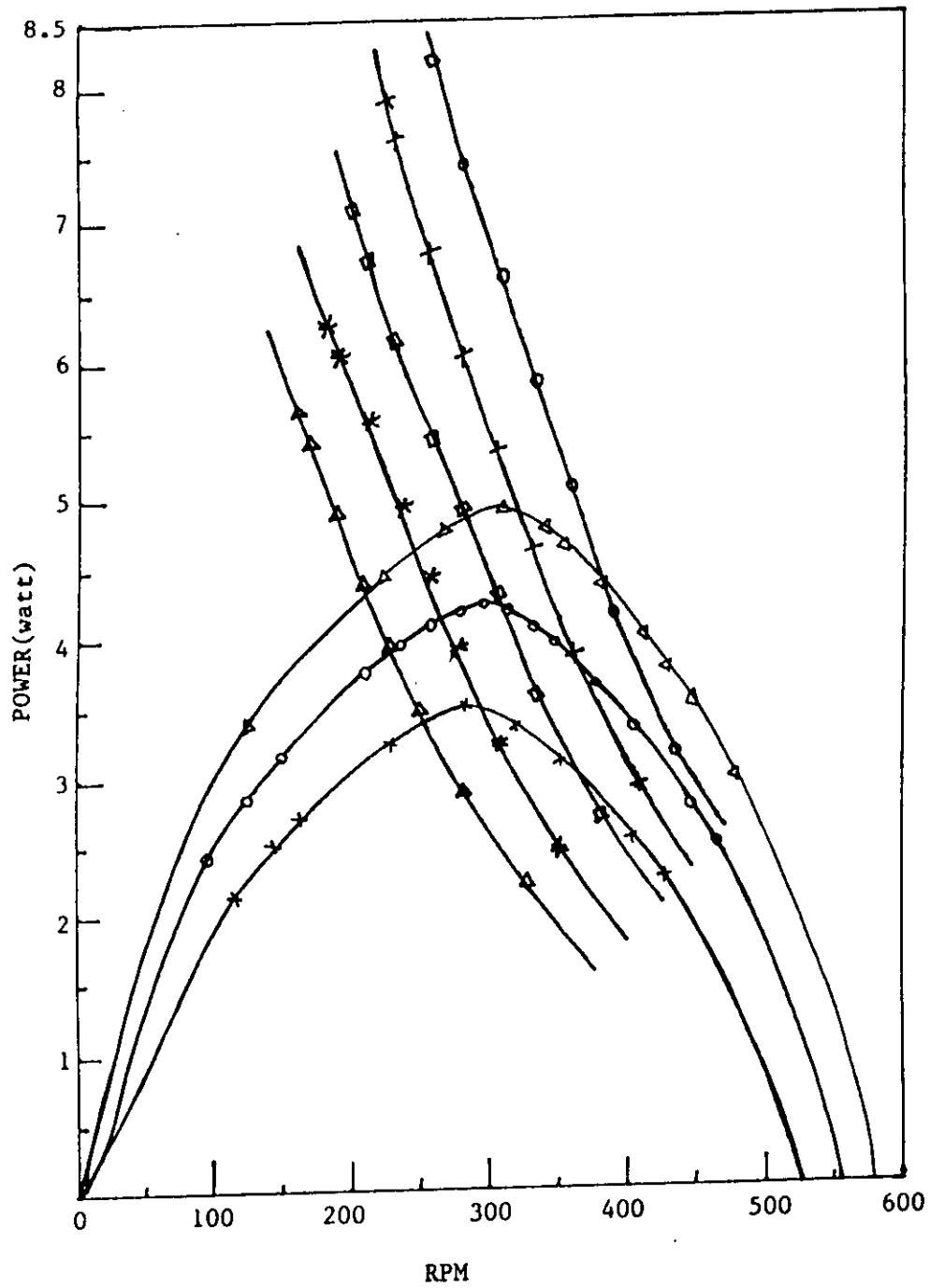
Figure 4.3.1: Comparison of different P-N characteristics of three bladed wind turbine with the different P-N characteristics of D. C. electric motor for different input voltage.

81
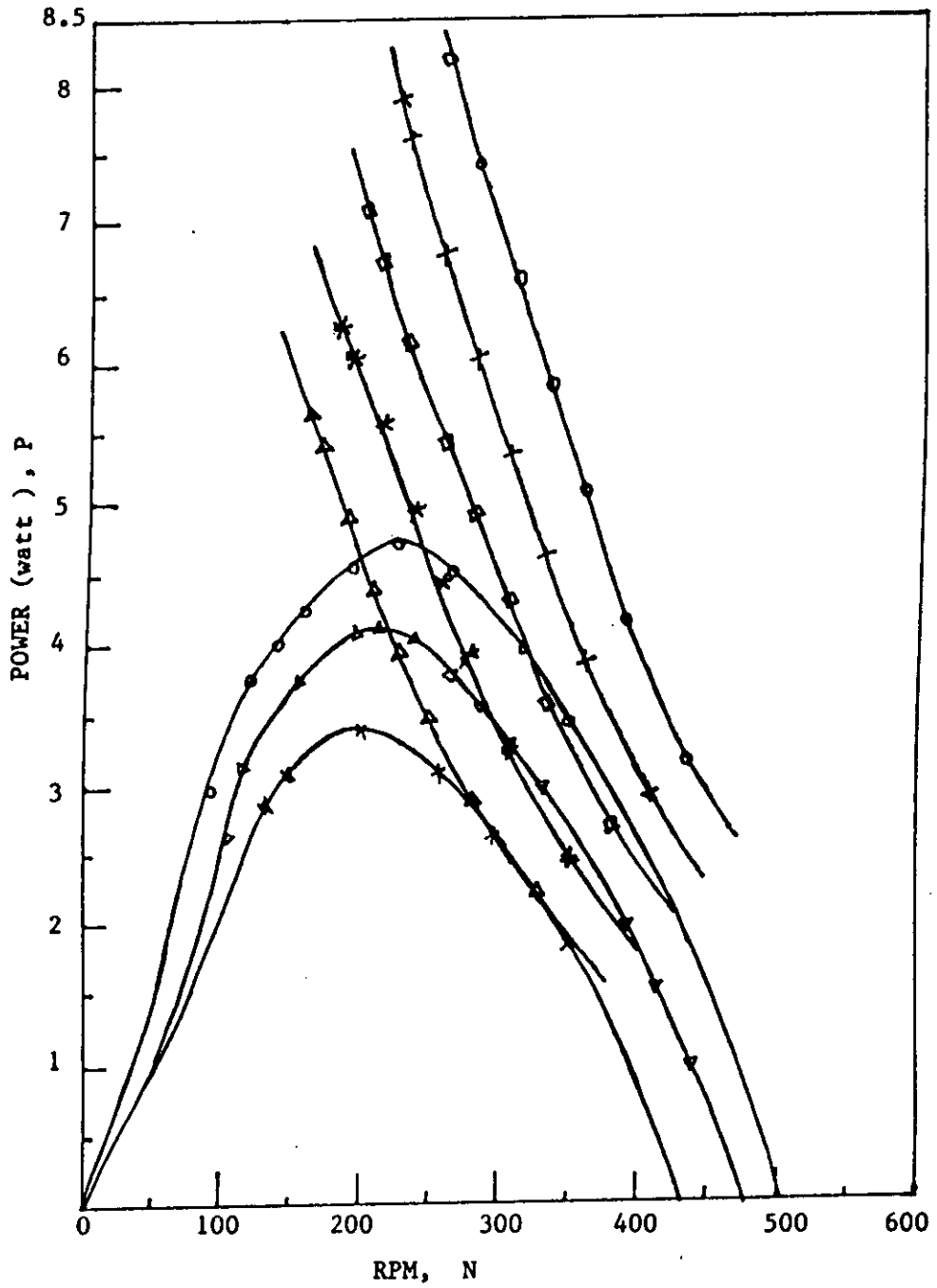
Figure 4.3.2: Comparison of different P-N characteristics of six bladed wind turbine with the different P-N characteristics of D. C. electric motor for different input voltage.
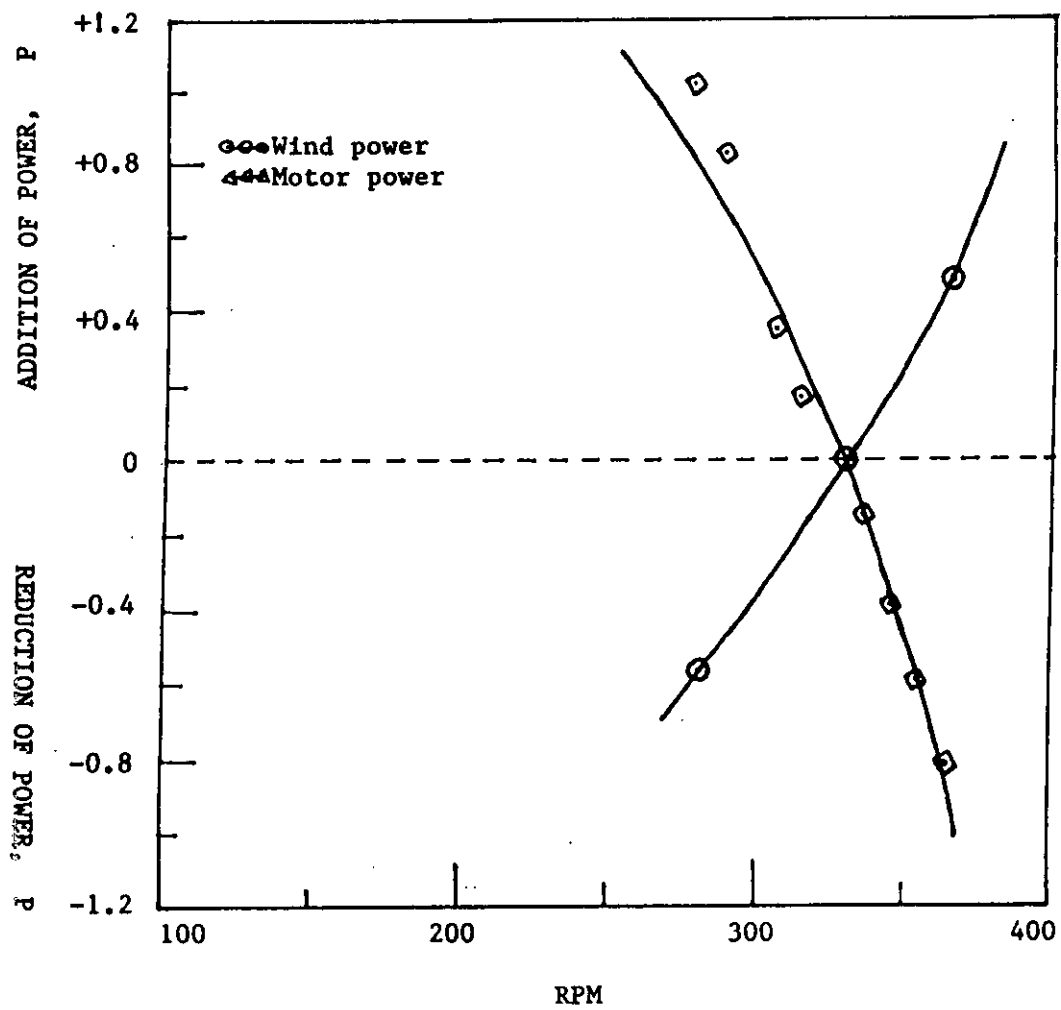
Figure 4.3.3: Comparison between the motor power variation to the three bladed wind turbine power variation for different wind velocity.
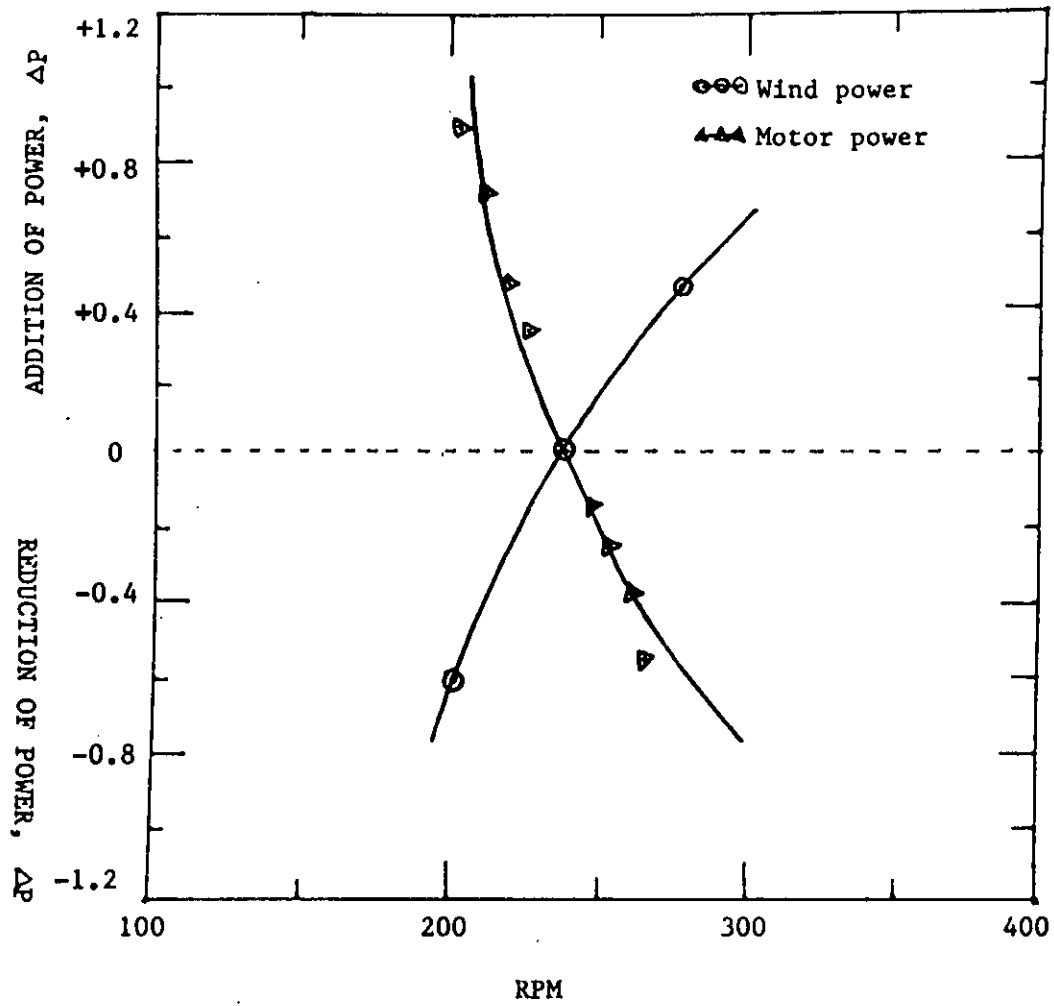
Figure 4.3.4: Comparison between the motor power variation to the six bladed wind turbine power variation for different wind velocity.

CHAPTER-5

RESULTS AND DISCUSSION

In this chapter, the results obtained are discussed. A brief discussion about the effect of basic parameters, such as the wind velocity, the tip speed ratio, the number of blades, the solidity of the wind turbine, the radius of the rotor, the type of airfoil on the behavior of horizontal axis wind turbine are presented in the following chapter for general information. The results of simulation system of the wind turbine are also discussed in this chapter.

The wind turbine extract power from the wind because it slows down the wind-not too much not too little. At standstill the turbine obviously produces no power and at very high rotational speeds the air is more or less blocked by the turbine and again no power is produced. Our laboratory specimen, on the basis of the present experiment, the three bladed wind turbine and the six bladed wind turbine were operated in between these two extremes so as to include the optimum values. These are shown in Figure 3.3.1 and Figure 3.3.2. In these figures, it is shown that the power of the wind turbine at any particular speed are depend on the wind velocity and the power of the turbine increases with the increase of the wind velocity. The maximum power of the wind turbine at different wind velocity are obtained at different rotational speed of the wind turbine. So, with the increase of wind velocity, the region of higher turbine power move to the region of higher values of the turbine speeds. Again it is also interesting to know the torque-speed curve of a wind turbine at different wind velocities. The torque is equal to the tangent of a line through the origin and some point of the P-N curve. In our experiment, it is shown that if the wind speed increases, the power and torque increase, so for each wind speed a

separate curve has drawn both for power and for torque and which are shown in Figure 3.3.3 and Figure 3.3.4. These groups of curves are rather inconvenient to handle as they vary with the wind speed V_∞, the radius R, of the turbine and even the density ρ, of the air. The immediate advantage is that the behavior of turbine at different wind velocities can be reduced to two curves Cp-λ and CT-λ. and the power coefficient (Cp), torque coefficient (C_T) variation with respect to tip speed ratio are shown in Figure 3.3.5 and Figure 3.3.6. The tip losses and the Hub losses depend on the tip speed ratio. For the lower design tip speed ratios, generally a high number of blades are chosen. This is done because the influence of number of blades on power coefficient is larger at lower tip speed ratios. For a high design tip speed ratio with a high number of blades will lead a very small and this blades which results in manufacturing problems and a negative influence on the lift and drag properties of blades. From the result of our laboratory experiment, increase of number of blades shows that the region of higher power coefficients move to the region of smaller values of tip speed ratio. The increased number of blades increases the cost of blade manufacture. The advantages of increasing the number of blades are improved performance and lower torque variation due to wind shear. The maximum power coefficient is also affected by the number of blades, because of the tip losses that occur at the tips of the blades. These losses depend on the number of blades. Increase of number of blades increases the solidity of the wind turbine. More the solidity of the turbine, the starting speed of the turbine will be less which is shown in Figure 3.3.7. It is seen that a high solidity turbine can be self starting, but there is still a dead band of very low torque around tip speed ratio λ. Peak torque drops as solidity is increased and increased solidity also requires larger, more expensive blades, so increased solidity is not an attractive solution to the self-starting problem.

The values of power coefficient (C_p) and drag coefficient (C_D) of a given airfoil vary with the wind speed. For wind turbine with higher tip speed ratios i.e. with smaller blades and smaller flow angle ϕ, the effect of wake rotation is much smaller. A finite number of blades, instead of the ideal infinite blade number, causes an extra reduction in power, particularly at low tip speed ratios. This is caused by the pressure leakage around the tip of the blade; the higher pressure at the front side of the airfoil and the lower pressure at the back side are short circuited at the tip of the blade causing a cross-flow around the tip, hence a decrease in pressure difference over the airfoil and a lift force approaching zero at the tip itself. The length-width ratio of the whole blade determines the influence of this tip loss, the higher this ratio the lower the tip losses.

In the simulation system, the system as developed by the d.c. motor is to simulate as nearly as possible the characteristics found from the experimental results as mentioned earlier. Since the electric motor have a different performance as shown in Figure 4.2.1 and it is loaded by brakes to achieve a power variation curve whose image is similar to the power variation curve due to variation of wind velocity. Because of the wind turbine power variation curve is the image of the power variation curve of the motor, any power fall of the wind turbine due to decrease of wind velocity can easily be compensated from the motor power or any power rise of the wind turbine due to increase of the wind velocity can easily be used through the motor for further utilization. By these way, the simulation system of the wind power can be used for research activities at the indoor laboratory condition avoiding completed and weather depended outdoor experimentation.

CHAPTER-6

CONCLUSIONS AND RECOMMENDATIONS

The main purpose of the study is to determine the different performance characteristics of wind turbine, to analyze the different performance characteristics and self-starting characteristics of three bladed wind turbine and six-bladed wind turbine, to compare the performance characteristics of wind turbine with the D.C motor characteristics and finally to simulate the wind turbine power by the D.C. motor.

From the present investigation the following conclusions may be drawn:

1. For the maximum power extraction from the wind turbine at particular wind velocity, it should be considered the turbine speed because at low turbine speed, the turbine produces less power and at very high rotational speeds, the air is more or less blocked by the turbine and again less power is produced.

2. The performance characteristics depend on the number of blade of the wind turbine. The area under the Cp-λ curve for six-bladed wind turbine is less than the area under the Cp-λ curve for three bladed wind turbine and the stability of the six-bladed wind turbine is more than the stability of the three bladed wind turbine. The maximum power region for six bladed wind turbine, can obtained at lower turbine speed than the three bladed wind turbine speed, so the optimum number of blade should be considered for better turbine performance and optimum stable turbine speed.

3. The values of power coefficient (C_p) and drag coefficient (C_D) for a given airfoil vary with the wind speed. Power losses due to drag can be reduced by increasing the turbine solidity and reducing tip speed. But only at expense of increased blade weight and cost. Improvements in airfoil lift to drag ratio will permit the reduced solidity and higher tip speeds. Increased tip speeds would be advantageous for reducing the capacity of the speed increaser gear needed to set-up the low turbine speed to the electrical motor speed. Although these trade-offs are complex, it will probably be necessary to sacrifice some aerodynamic efficiency to reduce blade size and weight of large wind turbines.

4. The wind turbine simulation system can be obtained experimentally by the electric motor. These simulation system can enhance the wind power utilization at different loading conditions. The loading conditions of the wind turbine are different as caompare to electric motor. Due to variation of wind power, the simulation system can ensure the proper utilization of the wind power. For these reason, the power simulation system should be considered at that loading conditions where the power variation are as usual.

This type of wind turbine power simulation system can be used for research activities at the indoor laboratory condition avoiding completed and weather depended outdoor experimentation. Studies of the future wind turbine power simulation system should-include an evaluation of the following fields:

Different IC chip can be used instead of mechanical brake on the motor shaft for the addition of power or reduction of power on the motor shaft. Again by these IC chip, a feed back can be response from the wind turbine shaft where

these have any power fall or rise due to wind velocity variation and these feed back can control the power addition or reduction of power on the motor shaft.

REFERENCES

1.   Golding, E. W., "The Generation of Electricity by Wind Power", Spon Ltd., London, 1995 and 1976.

2.   Eldridge, R. F., "Wind Machines", Van Nostrand Reinhold Company, 1980.

3.   Betz, A., "Cotinger Nachr", p. 193, 1919.

4.   Golding, S., "On the Vortex Theory of Screw Propellers", Proc. of Royal Soc., A123. 440, 1929.

5.   Theodorsen, T., "The Theory of Propellers, I-Determination of the Circulation Function and the Mass Coefficient for Dual-Rotating Propellers", NACA Report 775, 1944.

6.   Lock, C. N. H., "Note on the Characteristics Curve for an Airscrew or Helicopter", Aeronautical Research Council Reports and Memoranda No. 2673, June 1947.

7.   Lock, C. N. H. and Bateman H., "Some Experiments on Airscrews at Zero Torque, With Applications to a Helicopter Descending with the Engine Off, and to the Design of Windmills", Aeronautical Research Council Reports and Memoranda No. 885, September 1923.

8.   Glauert, H., "The Analysis of Experimental Results in the Windmill Brake and Vortex Ring States of an Airscrew" Aeronautical Research Council Reports and Memoranda No. 1026, February 1926.

9.   Gessow, A. and Myers, G. C. Jr., "Aerodynamics of the Helicopter", Frederick Ungar Publishing Co., New York, 1952.

10.   Johnson, W., "Helicopter Thoery", Princeton University Press, 1980, pp. 106.

11. Wilson, R. E., "Aerodynamic Potpouri", Proc. of the DOE/NASA Wind Turbine Dynamics Conference, February 1981, NASA CP-2185, DOE CONF-801226.

12. Yamane, T., Tsutsui, and Orita, T., "The Aerodynamic Performance of a Horizontal Axis Wind Turbine in Large Induced Velocity States", Proc. of the Fourth International Symposium on Wind Energy Systems, Stockhom, September 1984.

13. Anderson, M. B., "A Vortex-Wake Analysis of a Horizontal Axis Wind Turbine and a Comparison with a Modified Blade Element Theory", Proc. of the Third International Symposium on Wind Energy Systems, Copenhagen, August 1980.

14. Glasgow, J. C., Miller, D. and Sullivan, T., "Rotor Blade Bending Loads for MOD-O Experimental Wind Turbine", NASA PIR 163 October 1980.

15. Walker, S. N., "Performance and Optimum Design Analysis/Computation for Propeller Type Wind Turbines", Ph.D Thesis, Oregon State University, Oregon, May 1976.

16. Anderson, M. B., "Blade Shapes for Horizontal Axis Wind Turbines", Proc. of Second BWEA Wind Energy Workshop, Cranfield, April 1980.

17. Shepherd, D. G., "Note on a Simplified Approach to Design Point Performance Analysis on HAWT Rotors", Journal of Wind Engineering, Vol. 8, No. 2, 1984.

18. Jensen, W. A. M., "Horizontal Axis Fast Running Wind Turbines for Developing Countries", Steering Committee for Wind Energy in Developing Countries, P.O. Box 85, Amersfoort, The Netherland, June 1976.

19. Craig, A. G., "Fabrication of Extruded Vertical Axis Turbine Blades", NASA Conference Publication 2106, DOE Publication CONF-7904111.

20. Putman, P. C., "Power From the Wind", Van Nostrand Co., Inc. 1948, pp. 157-169.

21. Spera, D. A., "Structural Analysis of Wind Turbine Rotors for NSF-NASA MOD-O Wind Power System", NASA-Langley E-8133, 1975.

92

22. Glasgow, J. C., Miller, D. R. and Corrigan R. D., "Comparison of Upwind and Downwind Rotor Operations of the DOE/NASA 100-kW MOD-O Wind Turbine", Second DOE/NASA Wind Turbine Dynamics workshop, Cleveland, Ohio, February 24-26, 1981.

23. Linscott, B. S. and Glasgow, J. C., "Experimental Data and Theoretical Analysis of an Operating 100 kW Wind Turbine", Presented at the 12th International Energy Conversion Conference, Washington D. C., September 1977.s

24. Milborrow, D. J., "Performance, Blade Loads and Size Limits for Horizontal Axis Wind Turbines", Central Electricity Research Laboratories, Kelvin Avenue, Latherhead, Surrey.

25. Spera, D. A. and Janetzke, "Effects of Rotor Location, Coning and Tilt on Critical Loads in Large Wind Turbines", Wind Technology Journal, Vol. 1, No. 2, Summer 1977.

26. Powles, S. R. L., "The Effects of Tower Shadow on the Dynamics of a Horizontal Axis Wind Turbine", Journal of Wind Engineering. Vol. 7, No. 1, 1983.

27. Wilmshurst, S. M., Powels, S. J. R. and Wilson, D. M. A., "The Problem of Tower Shadow", Proc. of the Seventh BWEA Wind Energy Conference, Oxford 27-29 March 1985.

28. Wentz, W. H. and Snyder, M. H., "Feasibility Study of Aileron and Spoiler Control Systems for Large Horizontal Axis Wind Turbines", WER-10, Wind Energy Laboratory, wichita State University, November, 1979.

29. Lysen.E.H.,"Introduction to Wind Energy".

APPENDICES

APPENDIX-A

The following experimental data are for the three-bladed wind turbine:

Wind velocity, $V_1 = 4.2$ m/s

Blade length, $R = 30$ cm

Air density, $\rho_a = 1.1424$ kg/m^3

No. of Obs.	Lever length (inch)	Lever weight (OZ)	T torque (N-mm)	N (rpm)	P Power (watt)	C_P	λ	$C_T = \dfrac{C_P}{\lambda}$
1	3.0	2.4	50.87	461	2.456	0.205	3.45	5.94×10^{-2}
2	3.5	2.4	59.35	442	2.747	0.229	3.30	6.94×10^{-2}
3	4.5	2.4	76.31	400	3.296	0.270	3.00	9.0×10^{-2}
4	5.5	2.4	92.75	374	3.672	0.305	2.79	10.9×10^{-2}
5	6.5	2.4	110.71	340	3.942	0.328	2.54	12.91×10^{-2}
6	7.0	2.4	118.71	326	4.053	0.339	2.438	13.90×10^{-2}
7	7.5	2.4	127.19	310	4.127	0.345	2.318	14.88×10^{-2}
8	8.0	2.4	135.67	295	4.191	0.35	2.206	15.86×10^{-2}
9	8.5	2.4	144.15	275	4.151	0.346	2.05	16.87×10^{-2}
10	9.0	2.4	152.62	255	4.075	0.34	1.91	17.80×10^{-2}
11	9.5	2.4	161.10	231	3.897	0.326	1.73	18.80×10^{-2}
12	6.0	4.0	169.58	210	3.729	0.311	1.60	19.40×10^{-2}
13	7.0	4.0	197.85	151	3.129	0.261	1.13	23.10×10^{-2}
14	8.0	4.0	226.11	123	2.812	0.243	0.92	26.00×10^{-2}
15	9.0	4.0	254.57	98	2.444	0.223	0.75	29.80×10^{-2}

At no load condition, N = 550 rpm.

APPENDIX-B

The following experimental data are for the three-bladed wind turbine:

Wind velocity, $V_2 = 3.95$ m/s

Blade length, $R = 30$ cm

Air density, $\rho = 1.1424$ kg/m³

No. of Obs.	Lever length (inch)	Lever weight (OZ)	T torque (N-mm)	N (rpm)	P Power (watt)	C_P	λ	$C_T = \dfrac{C_P}{\lambda}$
1	-	-	0	520	0	0	-	0
2	3.0	2.4	50.87	423	2.25	0.225	3.36	6.69×10^{-2}
3	3.5	2.4	59.35	400	2.5	0.251	3.14	8.0×10^{-2}
4	5.0	2.4	84.79	345	3.06	0.307	2.74	11.2×10^{-2}
5	6.0	2.4	101.23	315	3.34	0.335	2.51	13.35×10^{-2}
6	7.0	2.4	118.71	280	3.48	0.349	2.226	15.68×10^{-2}
7	8.0	2.4	135.67	225	3.20	0.321	1.71	16.77×10^{-2}
8	9.5	2.4	161.10	160	2.70	0.271	1.27	21.34×10^{-2}
9	6.0	4.0	169.58	141	2.504	0.251	1.12	22.40×10^{-2}
10	6.5	4.0	183.70	112	2.155	0.216	0.89	24.26×10^{-2}

At no load condition the rpm of turbine = $N_0 = 520$

APPENDIX-C

The following experimental data are for the three-bladed wind turbine:

Wind velocity, V_3 = 4.40 m/s

Blade length, R = 30 cm

Air density, ρ = 1.1424 kg/m^3

No. of Obs.	Lever length (inch)	Lever weight (OZ)	T torque (N-mm)	N (rpm)	P Power (watt)	C_P	λ	$C_T = \dfrac{C_P}{\lambda}$
1	-	-	0	575	0	0	-	-
2	3.5	2.4	59.35	475	2.960	0.215	3.39	6.34×10^{-2}
3	4.5	2.4	76.31	439	3.511	0.255	3.13	8.15×10^{-2}
4	5.0	2.4	84.79	423	3.750	0.272	3.02	9.01×10^{-2}
5	5.5	2.4	93.75	406	3.98	0.289	2.91	9.93×10^{-2}
6	6.5	2.4	110.71	375	4.35	0.316	2.68	11.8×10^{-2}
7	7.5	2.4	127.10	346	4.626	0.335	2.47	13.6×10^{-2}
8	8.0	2.4	135.67	333	4.73	0.343	2.47	13.9×10^{-2}
9	9.0	2.4	152.62	305	4.801	0.348	2.18	16.0×10^{-2}
10	6.0	4.0	169.58	261	4.627	0.336	1.86	18.1×10^{-2}
11	6.5	4.0	183.70	224	4.351	0.312	1.60	19.5×10^{-2}
12	9.0	4.0	254.37	124	3.305	0.24	0.885	27.0×10^{-2}

At no load condition, N = 575 rpm.

APPENDIX-D

The following experimental data are for the six-bladed wind turbine:

Wind velocity, $V_1 = 4.2$ m/s

Blade length, R = 30 cm

Air density, $\rho = 1.1424$ kg/m^3

No. of Obs.	Lever length (inch)	Lever weight (OZ)	T torque (N-mm)	N (rpm)	P Power (watt)	C_P	λ	$C_T = \dfrac{C_P}{\lambda}$
1	0	0	0	470	0	-	-	-
2	3.0	2.4	50.87	390	2.05	0.174	2.917	5.97×10^{-2}
3	5.0	2.4	84.79	334	2.97	0.248	2.50	9.92×10^{-2}
4	6.0	2.4	101.23	307	3.258	0.272	2.30	11.82×10^{-2}
5	7.0	2.4	118.71	286	3.545	0.296	2.14	13.83×10^{-2}
6	8.0	2.4	135.67	267	3.785	0.316	2.00	15.80×10^{-2}
7	9.5	2.4	161.10	237	4.047	0.337	1.775	18.99×10^{-2}
8	6.5	4.0	183.70	214	4.117	0.344	1.60	21.50×10^{-2}
9	7.0	4.0	197.83	198	4.096	0.342	1.48	23.11×10^{-2}
10	7.5	4.0	211.96	179	3.973	0.332	1.34	24.78×10^{-2}
11	8.0	4.0	226.11	158	3.712	0.31	1.18	26.27×10^{-2}
12	9.0	4.0	254.37	117	3.114	0.26	0.88	29.55×10^{-2}
13	10.0	4.0	282.64	99	2.93	0.2445	0.74	0.33×10^{-2}

At no load condition, N = 470 rpm.

APPENDIX-E

The following experimental data are for the six-bladed wind turbine:

Wind velocity, $V_2 = 3.95$ m/s

Blade length, $R = 30$ cm

Air density, $\rho = 1.1424$ kg/m^3

No. of Obs.	Lever length (inch)	Lever weight (OZ)	T torque (N-mm)	N (rpm)	P Power (watt)	C_P	λ	$C_T = \dfrac{C_P}{\lambda}$
1	0	0	0	425	0	-	-	-
2	3.0	2.4	50.87	350	1.860	0.187	2.78	6.73 x 10^{-2}
3	5.0	2.4	84.79	297	2.630	0.264	2.36	11.19 x 10^{-2}
4	7.0	2.4	118.71	252	3.130	0.3145	2.00	15.73 x 10^{-2}
5	9.5	2.4	161.10	200	3.425	0.344	1.60	21.50 x 10^{-2}
6	7.0	4.0	197.85	150	3.050	0.311	1.19	26.13 x 10^{-2}
7	7.5	4.0	211.96	130	2.850	0.281	1.04	27.02 x 10^{-2}
8	8.0	4.0	226.49	110	2.610	0.261	0.88	29.66 x 10^{-2}
9	10.0	4.0	282.64	77	2.250	0.226	0.61	-37.05 x 10^{-2}
10	11.0	4.0	310.9	65	2.114	0.225	0.514	43.77 x 10^{-2}

At no load condition, N = 425 rpm.

APPENDIX-F

The following experimental data are for the six-bladed wind turbine:

Wind velocity, V_3 = 4.40 m/s

Blade length, R = 30 cm

Air density, ρ = 1.1424 kg/m^3

No. of Obs.	Lever length (inch)	Lever weight (OZ)	T torque (N-mm)	N (rpm)	P Power (watt)	C_P	λ	$C_T = \dfrac{C_P}{\lambda}$
1	0	0	0	500	0	-	-	-
2	5.5	2.4	93.75	350	3.415	0.248	2.50	9.92 x 10^{-2}
3	7.0	2.4	118.71	312	3.950	0.282	2.23	12.65 x 10^{-2}
4	9.5	2.4	161.10	266	4.489	0.326	1.90	17.16 x 10^{-2}
5	7.0	4.0	197.83	225	4.736	0.344	1.60	21.50 x 10^{-2}
6	8.0	4.0	226.11	192	4.546	0.334	1.37	24.38 x 10^{-2}
7	9.0	4.0	254.37	159	4.25	0.308	1.16	26.55 x 10^{-2}
8	11.0	4.0	310.90	109	3.551	0.256	0.780	32.82 x 10^{-2}

APPENDIX - G

The following data are obtained after testing the D. C. Electric Motor at 32 Volt AC.

DATA TABLE

No. of Observation	Dead wt. (OZ)	Lever Length (inch)	Torque (N-mm)	Speed (rpm)	Power (Watt)
1	2.4	4	67.83	316	2.24
2	2.4	5	84.79	297	2.65
3	2.4	6	101.75	277	2.95
4	2.4	8	135.68	247	3.51
5	2.4	10	169.58	224	3.95
6	2.4	12	203.50	205	4.35
7	4.0	9	259.38	185	4.93
8	4.0	11	310.91	16.5	5.38
9	4.0	12	339.17	160	5.68

APPENDIX - H

The following data are obtained after testing the D. C. Electric Motor at 36 Volt AC.

DATA TABLE

No. of Observation	Dead wt. (OZ)	Lever Length (inch)	Torque (N-mm)	Speed (rpm)	Power (Watt)
1	2.4	4	67.83	350	2.48
2	2.4	6	101.75	305	3.25
3	2.4	8	135.67	275	3.91
4	2.4	10	169.58	252	4.48
5	2.4	12	203.50	232	4.95
6	2.4	9	254.38	210	5.59
7	4.0	11	310.91	187	6.08
8	4.0	12	339.17	178	6.32

APPENDIX - I

The following data are obtained after testing the D. C. Electric Motor at 40 Volt AC.

DATA TABLE

No. of Observation	Dead wt. (OZ)	Lever Length (inch)	Torque (N-mm)	Speed (rpm)	Power (Watt)
1	2.4	4	67.83	380	2.70
2	2.4	6	101.75	335	3.57
3	2.4	8	135.67	303	4.30
4	2.4	10	169.58	278	4.93
5	2.4	12	203.50	255	5.45
6	2.4	9	254.38	230	6.13
7	4.0	11	310.91	208	6.77
8	4.0	12	339.17	200	7.10

APPENDIX - J

The following data are obtained after testing the D. C. Electric Motor at 44 Volt AC.

DATA TABLE

No. of Observation	Dead wt. (OZ)	Lever Length (inch)	Torque (N-mm)	Speed (rpm)	Power (Watt)
1	2.4	4	67.83	407	2.91
2	2.4	6	101.75	360	3.84
3	2.4	8	135.67	327	4.65
4	2.4	10	169.58	302	5.36
5	2.4	12	203.50	283	6.03
6	2.4	9	254.38	255	6.79
7	4.0	11	310.91	234	7.61
8	4.0	12	339.17	225	7.97

APPENDIX - K

The following data are obtained after testing the D. C. Electric Motor at 48 Volt AC.

DATA TABLE

No. of Observation	Dead wt. (OZ)	Lever Length (inch)	Torque (N-mm)	Speed (rpm)	Power (Watt)
1	2.4	4	67.83	440	3.12
2	2.4	6	101.75	390	4.15
3	2.4	8	135.67	357	5.07
4	2.4	10	169.58	330	5.86
5	2.4	12	203.50	310	6.60
6	2.4	9	254.38	278	7.41
7	4.0	11	310.91.	253	8.24

The experiment on the wind turbine are to be carried out of the following atmospheric condition:

Height of Mercury Column = 75 cm

So Atmospheric pressure $P_a = \dfrac{75}{100} \times 13.6 \times 9810$

$$p_a = 10^5 N/m^2$$

Atmospheric temperature, $t_a = 32^oC$

Gas constant, $R_g = 287$ J/kj^{o}K

Air density, $\quad p_a = \dfrac{P_a}{RT} = \dfrac{10^5}{297 \times (32+273)}$

$$\therefore p_a = 1.1424 \ kg/m^3$$